

# UNCLASSIFIED

AD NUMBER
AD826033
NEW LIMITATION CHANGE
TO Approved for public release, distribution unlimited
FROM Distribution authorized to U.S. Gov't. agencies and their contractors; Critical Technology; NOV 1967. Other requests shall be referred to Naval Electronic Systems Command, Code 05143, Washington, DC 20360.
AUTHORITY
nesc ltr, 11 aug 1971

THIS PAGE IS UNCLASSIFIED

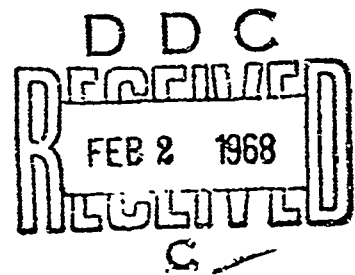
AD826033

FINAL ENGINEERING REPORT  
for  
DEVELOPMENT AND FABRICATION OF  
SOLID-STATE HIGH-SPEED OPTICAL DETECTORS

This Report Covers the Period  
16 May 1966 through 30 September 1967

Texas Instruments Incorporated  
13500 North Central Expressway  
Dallas, Texas 75222

Navy Department  
Bureau of Ships  
Electronics Division



Contract No. NObsr 95337  
Project No. SF021-02-01  
Task No. 9349

November 1967

STATEMENT #2 UNCLASSIFIED

This document is subject to special export controls and export transmittal to foreign governments or foreign nationals may be made only with prior approval of *Naval Electronic Systems Command*, Code-05143, Washington, D.C. 20360

Report No. 03-67-104

FINAL ENGINEERING REPORT  
for  
DEVELOPMENT AND FABRICATION OF  
SOLID-STATE HIGH-SPEED OPTICAL DETECTORS

This Report Covers the Period  
16 May 1966 through 30 September 1967

Texas Instruments Incorporated  
13500 North Central Expressway  
Dallas, Texas 75222

Navy Department  
Bureau of Ships  
Electronics Division

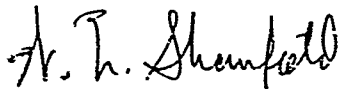
Contract No. N0bsr 95337  
Project No. SF021-02-01  
Task No. 9349

November 1967

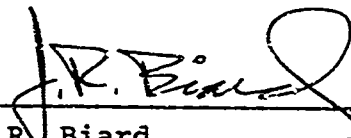
ABSTRACT

The development, fabrication, and characterization of a high-speed silicon avalanche photodiode for 0.9  $\mu\text{m}$  are described. Two structures, an NP $\pi$ P and a graded-guardring N $^+$ P structure, were fabricated. On the planar NP $\pi$ P structure, edge breakdown was found to be a problem of structures having wide  $\pi$ -regions. Since wide depletion layer widths are required for high ac quantum efficiency at 0.9  $\mu\text{m}$ , effort was shifted entirely to the N $^+$ P structure.

Final characterization showed that all the N $^+$ P diodes delivered had low-noise avalanche gains greater than 160, with many diodes exhibiting gains greater than  $10^3$ . The diodes typically have a series resistance of 50 ohms, junction capacitance of 1.3 pF, noise slope of 2.5 or less, ac quantum efficiency of 35 percent, bulk leakage current of 0.5 nA, and a breakdown voltage of 170 volts. The NEP of a 30-MHz bandwidth photodetector system was found to measure  $2 \times 10^{-13} \text{ W Hz}^{-1/2}$  at an optimum gain of 160--a factor of 100 improvement over a non-avalanching photodetector.



W. N. Shaunfield  
Project Engineer



J. R. Biard  
Program Manager

TABLE OF CONTENTS

SECTION	TITLE	PAGE
I.	TECHNICAL REVIEW . . . . .	1
A.	Purpose . . . . .	1
B.	General Factual Data. . . . .	2
C.	Detailed Factual Data . . . . .	2
	1. Device Design and Fabrication. . . . .	2
	a. General . . . . .	2
	b. NP $\pi$ P Structure. . . . .	3
	c. N $^+$ P Structure . . . . .	12
	d. Package and Diode Mount . . . . .	15
	2. Device Characterization. . . . .	17
	a. Gain Characteristics. . . . .	17
	b. Quantum Efficiency. . . . .	22
	c. Leakage Currents. . . . .	30
	d. Avalanche Noise . . . . .	32
	e. Equivalent Circuit. . . . .	33
	f. Frequency Limitations . . . . .	35
	g. NEP . . . . .	37
	3. Project Performance and Schedule . . . . .	43
	D. Conclusions . . . . .	44
II.	PROGRAM FOR NEXT INTERVAL. . . . .	45
III.	REFERENCES . . . . .	47

LIST OF ILLUSTRATIONS

FIGURE	TITLE	PAGE
1.	Planar Epitaxial NP $\pi$ P Avalanche Multiplication Photodiode . . . . .	4
2.	Electric-Field Distribution in NP $\pi$ P Avalanche Multiplication Photodiode . . . .	5
3.	Simplified Representation of Electric Field at Junction Edge. . . . .	8
4.	Relative Photoresponse Across Surface of NP $\pi$ P Structure for Different Bias Voltages . . . . .	11
5.	Graded-Guardring Avalanche Photodiode. . . . .	13
6.	Composite Photomask Layout for Graded- Guardring Avalanche Photodiode. . . . .	14
7.	Photoresponse Across Surface of Graded- Guardring Structure . . . . .	16
8.	Coaxial Pill Package . . . . .	17
9.	BNC Diode Mount. . . . .	18
10.	TO-18 Package. . . . .	19
11.	Low-Frequency Gain and Noise Measurement Circuit . . . . .	21
12.	Avalanche Gain versus Bias Voltage for Typical N <sup>+</sup> P Diode at 0.9 $\mu$ m . . . . .	22
13.	I/M versus Voltage at 0.9 $\mu$ m . . . . .	23
14.	$\eta$ versus Voltage at 0.9 $\mu$ m . . . . .	24
15.	Breakdown Voltage versus Temperature . . . . .	25
16.	Automatic Bias Circuit . . . . .	26
17.	Typical Electron Quantum Efficiency for N <sup>+</sup> P Diode . . . . .	27
18.	Gain at 0.9 $\mu$ m versus Gain at 0.6328 $\mu$ m. . . . .	29
19.	Frequency Response of Quantum Efficiency . . . .	30
20.	Total Leakage Current versus Gain. . . . .	32
21.	Avalanche Noise Voltage versus Gain. . . . .	34

LIST OF ILLUSTRATIONS

FIGURE	TITLE	PAGE
22.	Avalanche Photodiode Equivalent Circuit. . . . .	35
23.	AC versus DC Gain. . . . .	38
24.	Preamplifier Circuit . . . . .	40
25.	NEP versus Gain for Diode No. 15 . . . . .	41
26.	Measured NEP versus Gain for Diode No. 18. . . . .	42

SECTION I  
TECHNICAL REVIEW

A. PURPOSE

Texas Instruments has conducted a program of development aimed at fabricating photodiodes which satisfy the following goals:

- 1) A photodiode will be developed which utilizes the avalanche mechanism.
- 2) The detector will be optimized to operate at 0.9- $\mu$ m wavelength.
- 3) Design goals for the detector will be a response of 0.15 ns with a sensitivity equal to or better than that of a photomultiplier tube used at the same wavelength.
- 4) The photodiodes will operate at and above room temperature and will not be affected by 100°C storage temperature.
- 5) The photodiodes will be capable of providing amplification of 100 or greater.

The program consisted of two phases: I, design and fabrication of the avalanche photodiodes; II, testing and characterization. Phase II began upon completion of the first diffusion runs to determine whether any modifications in the original design were necessary to achieve the desired characteristics. Specific steps of the complete program were:

- 1) Obtain photomasks
- 2) Determine optimum diffusions
- 3) Produce experimental epitaxial slices
- 4) Fabricate experimental planar diodes
- 5) Characterization of experimental diodes, including quantum efficiency, gain characterization, noise performance, and frequency response.



B. GENERAL FACTUAL DATA

Personnel and Hours Worked, Third Quarter

<u>Professional</u>	<u>Hours</u>
W. N. Shaunfield	332.0
Jim Lewis	2.0
Total Professional	334.0
 <u>Technician</u>	
Jerry Reid	465.0
Pauline Harris	10.0
Total Technician	475.0

C. DETAILED FACTUAL DATA

1. Device Design and Fabrication

a. General

An avalanche photodiode is a semiconductor junction photodiode designed to utilize the avalanche multiplication effect to achieve a signal current gain in the detector. When used in a photodetector system in which sensitivity is normally limited by noise in the preamplifier, avalanche gain offers an improved system sensitivity.

During the course of this effort, two silicon avalanche photodiode structures were investigated. Initially an  $\text{NP}^+\text{P}$  structure was considered; however, some inherent limitations of this structure were discovered, and effort was abandoned in favor of the simpler  $\text{N}^+\text{P}$  structure. This structure, utilizing a graded guardring, was successfully fabricated with gains typically over  $10^3$ . Each of the two structures is discussed in the following paragraphs.

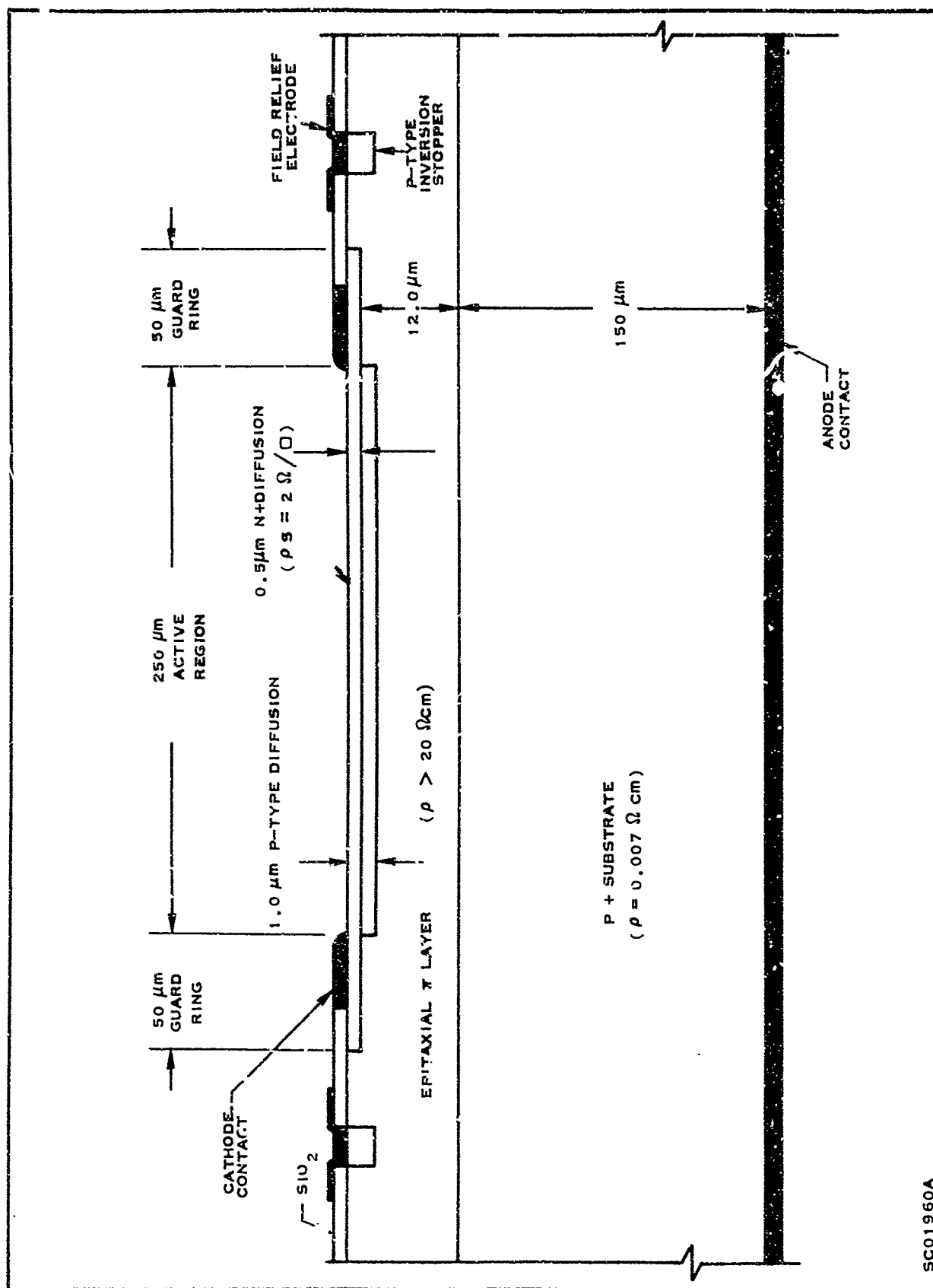
b. NP $\pi$ P Structure

A cross-section of the NP $\pi$ P structure is shown in Figure 1. The diode was fabricated using standard silicon planar epitaxial techniques as listed in the following order:

- 1) Grow  $\pi$  (low-concentration P-type) epitaxial layer on high-concentration substrates.
- 2) Diffuse P-type dopant (boron) in center active region and inversion-stopper ring.
- 3) Diffuse N-type dopant (phosphorus) in active region and guardring.
- 4) Apply front and back contacts.

Operation of the diode is best understood by considering the typical electric field at breakdown as seen in Figure 2. Normally, in a single planar diffusion, avalanche breakdown occurs at the edge due to the increased flux density and higher electric field at the sharp diode edge. Introducing the P-diffusion in the active region of the NP $\pi$ P structure produces a sharp spike in the electric field at the junction, as shown by the solid line in Figure 2. It was expected that this spike would cause the breakdown voltage to be lower here than on the junction edge. Neglecting the effects of radius of curvature at the N-diffusion edge, the electric field for the guardring is shown by the dashed line in Figure 2.

During operation, light entering the surface is absorbed throughout the bulk in an exponentially decreasing manner. For each photon absorbed an electron-hole pair is created. Electrons absorbed in the depletion region between 0 and  $X_2$  are swept to the junction at the electron saturated drift velocity by the high electric field. At the junction the electrons experience avalanche multiplication. Normally the reverse bias voltage is adjusted to a value just below sustained avalanche breakdown.



SC01960A

Figure 1. Planar Epitaxial NPTP Avalanche Multiplication Photodiode

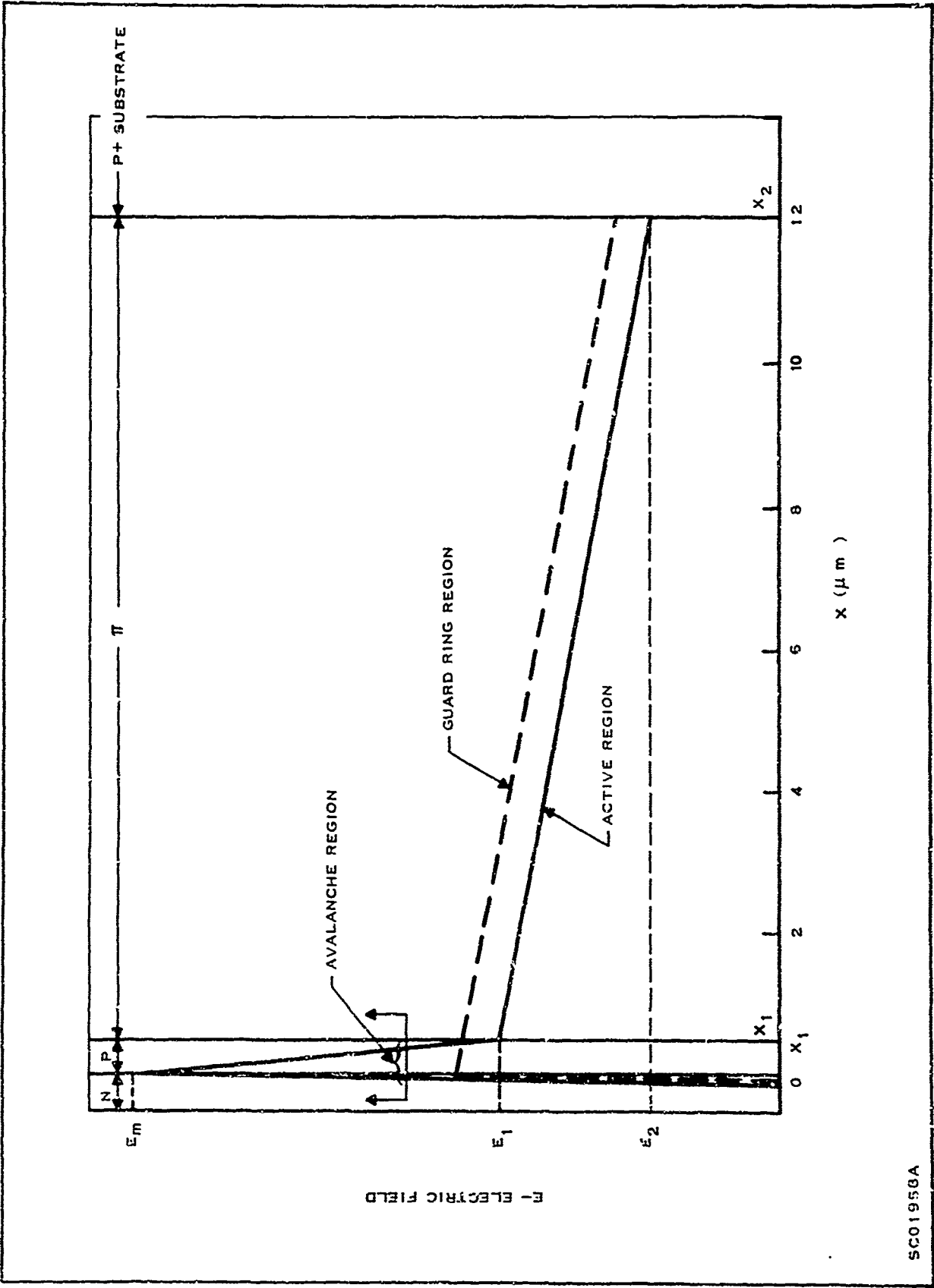


Figure 2. Electric-Field Distribution in NPTP Avalanche Multiplication Photodiode

The structure was chosen so that electrons instead of holes would be generated in the high field region and swept to the avalanche region. In silicon the higher electron ionization rate yields an electron gain much higher than the hole gain.

Calculations made to determine acceptable ranges for the impurity concentrations <sup>1/</sup> showed that the acceptable range of the P-diffusion concentration,  $N_p$ , was very critical ( $3 \times 10^{16}$  to  $6 \times 10^{16} \text{ cm}^{-3}$ ). Diodes were fabricated with the required impurity concentrations, as verified by using the capacitance-voltage technique for determining impurity concentration.<sup>2/</sup> However, all of the diodes fabricated had edge breakdown, occurring before the electric field in the active region had reached sufficient magnitude to give appreciable gain. The continued result of edge breakdown prompted a further investigation of the edge electric field.

In the calculations on required impurity concentrations the effect of junction curvature on the electric field was neglected. Along the edge of the planar-diffused junction a cylindrical junction is formed with radius approximately equal to junction depth. As a result the electric field is greater than in a plane junction, and breakdown voltage is reduced. For the case where the junction depth is small compared to depletion width the breakdown voltage is significantly reduced.<sup>3/</sup>

For the case where depletion width extends to a  $P^+$  substrate, as in the NPTP structure, edge effects are not as significant. This can be illustrated graphically if several simplifying assumptions are made:

- 1) Assume that the depletion region can be represented by a capacitor with plates separated by the plane junction depletion layer width.
- 2) Assume that there is no charge between the plates.

Assumption 1 is not valid, since the depletion width of the cylindrical junction is not as wide as that of a plane junction for the

same applied bias; neither is assumption 2, since there is charge in the depletion region.

Although these assumptions are not valid for a depletion region, they do allow the effects of a  $P^+$  substrate on the peak electric field to be illustrated by the graphical field-mapping technique. It should be pointed out that, although the field in a PN junction could be graphically mapped, the complication would not add to understanding of the effect.

Using the assumptions above, the electric field for a diffused junction is shown in Figure 3a. Note that the highest electric field, represented by close spacing of the flux lines, occurs at the junction edge. In Figure 3b the field is shown for the same potential applied to a junction with a  $P^+$  substrate under the  $N^+$ -diffusion. Note that the electric field at junction edge is not appreciably changed, while that at the plane portion of the junction is significantly increased. Ratio of edge breakdown voltage to center breakdown voltage would be much less in (b) than in (a).

In the NP $\pi$ P structure the peaking of electric field in the active region is further aided by the P-diffusion; however, the edge effect puts closer limits on the already critical dimensions. To prevent edge breakdown in the NP $\pi$ P structure it is necessary that the epitaxial layer width be small compared to breakdown depletion layer width in a concentration equal to that of the epitaxial layer. This requirement is contradictory to the wide epitaxial layer widths required for high quantum efficiency at 0.9  $\mu$ m and the impurity concentrations possible with epitaxial techniques. It is felt that the NP $\pi$ P structure would probably work with the concentrations and dimensions discussed in the first quarterly report; however, this would require extremely accurate control of diffusions.

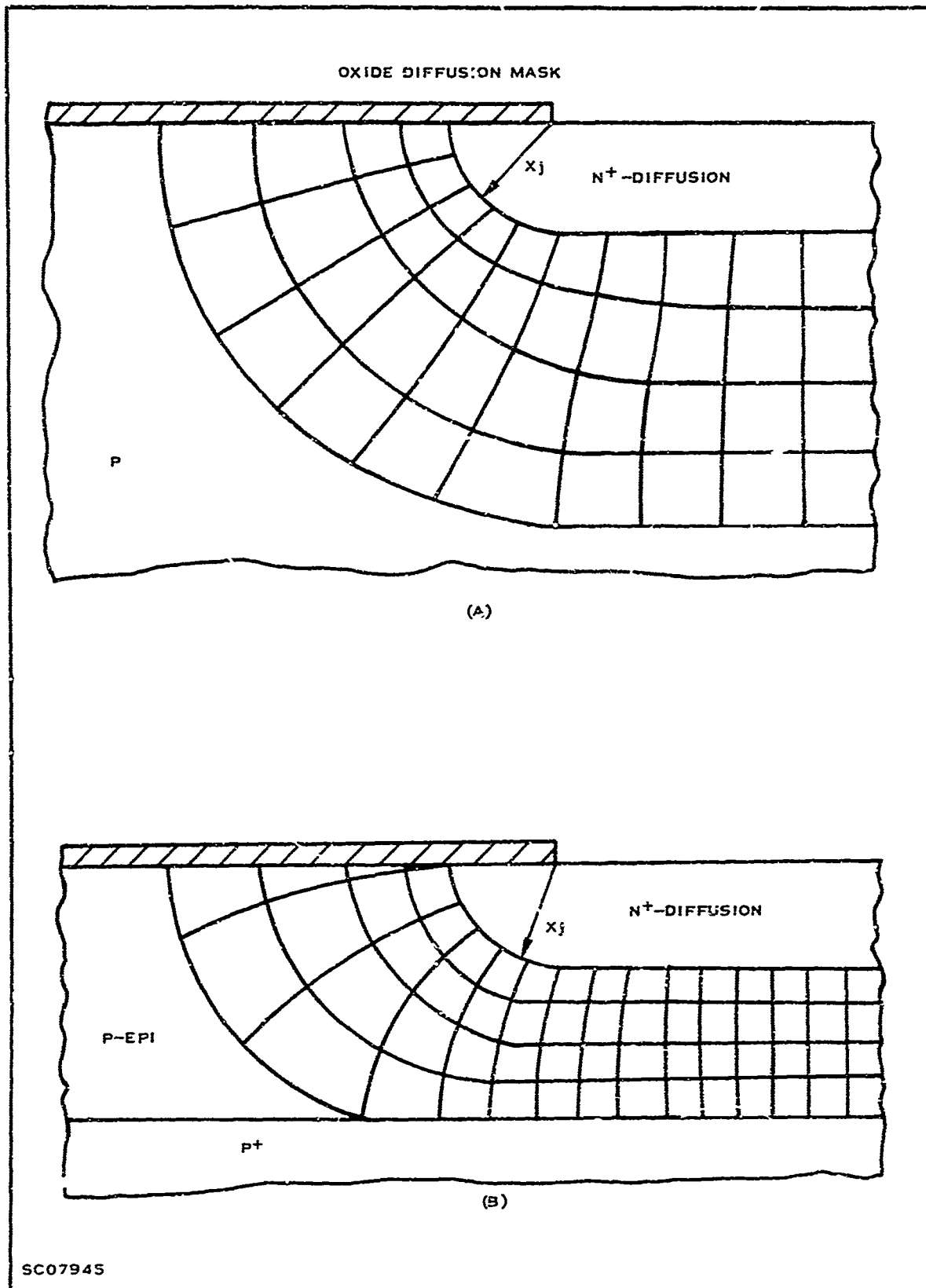


Figure 3. Simplified Representation of Electric Field at Junction Edge

Two additional techniques can be employed to reduce edge effects in the NP $\pi$ P structure. The first is to make the N-diffusion deeper. This results in a larger radius of curvature at the junction edge, reducing the peak electric field. There would be a reduction in quantum efficiency. The other technique would be to etch a moat into the region which normally is depleted at the junction edge. If there were no material to be depleted the electric field could not rise to the high value normally at the edge. However, the etched surface could result in high leakage currents.

A large portion of the contract effort was spent in the reduction of surface leakage currents. The lightly doped  $\pi$ -layer at the diode surface is very susceptible to surface conditions and almost always inverts to N-type for  $\pi$ -concentrations of  $10^{15} \text{ cm}^{-3}$  and less. These thin inversion layers on the diode surface were found to be the cause of high leakage currents.

The original design of the photomask included a P-type inversion-stopper ring which was diffused with the P-diffusion in the active region. However, the impurity concentration required in the active area proved to be too low for the inversion-stopper ring to be completely effective. Surface concentration of the P-diffusion is approximately  $10^{17} \text{ cm}^{-3}$ , while that required for the inversion stopper is  $5 \times 10^{18} \text{ cm}^{-3}$ . Two possible solutions were considered:

- 1) Perform a separate P<sup>+</sup>-diffusion in the ring.
- 2) Alloy an aluminum contact to the existing diffusion.

Aluminum, which is a P-type dopant in silicon, when alloyed to the ring should prevent inversion layers from forming over the inversion-stopper ring. The second approach was tried first, since this could be done during application of contacts and would not require an additional processing step.



The additional photomask required for the aluminum ring was received during the second quarter, and several runs were made with this approach. Results were not as good as expected. Leakage current was high, and there was drifting of the current with time at high reverse-bias voltages.

Traces made with an optical microprobe showed that under reverse bias an inversion layer was formed under the aluminum inversion-stopper ring. In making an optical-microprobe trace the diode is contacted between the P-contact on the back of the slice and the N-contact on the active region, and the photocurrent due to a 0.2-mil-diameter spot of light traced across the surface of the diode is measured. In addition the light is modulated at 400 Hz and the current is synchronously demodulated to avoid errors due to dark leakage currents. Magnitude of the signal versus distance is plotted on an X-Y recorder.

Figure 4 shows several plots made at different bias voltages on a diode with the aluminum inversion-stopper ring. The large photoresponse between the  $N^+$ -diffusion and the inversion-stopper aluminum indicates that inversion layers are present on the surface. The diode formed by the N-type inversion layer and the  $\pi$ -type bulk is light sensitive like a conventional diode. Note that at 2.0 volts bias the inversion-stopper ring is effective in isolating the diode's active region from the inversion layer outside inversion-stopper ring. However, as reverse bias is increased, photoresponse is observed outside the ring, indicating formation of an inversion layer under the ring connecting the inside and outside inversion layers. Inversion-layer photoresponse outside is lower than inside, apparently because of series resistance under the ring. Note that photoresponse falls off where the oxide was removed along the scribe line, indicating that this removal reduces the inversion layer's adverse effect. At bias voltages near breakdown (180 to 240 V) the leakage current was still too large, being typically 200  $\mu$ A.

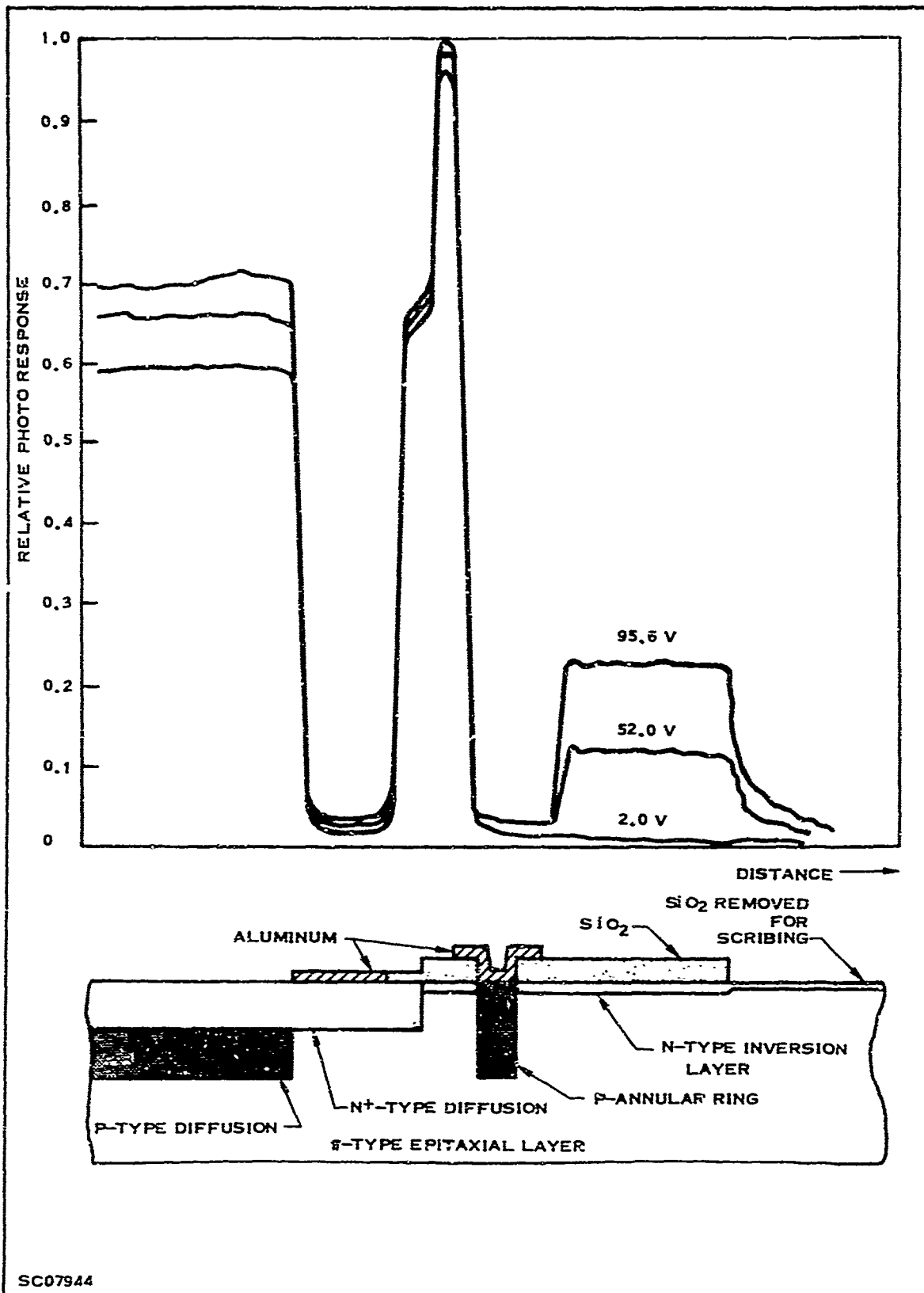


Figure 4. Relative Photoresponse Across Surface of NP $\pi$ P Structure for Different Bias Voltages

Because of the problem with aluminum alloyed to the P-ring, the other approach, requiring a separate  $P^+$ -diffusion, was tried. Although an additional processing step is necessary the diffusion is not critical. A photomask with only the inversion-stopper ring was obtained, and several runs were fabricated by this method. Results were very encouraging. An optical-microprobe trace showed no photoresponse outside the ring, and leakage currents typically were less than 100 nA at 150 volts bias. In addition no drifting of the leakage current was observed. The separate  $P^+$ -diffusion was included in the  $N^+P$  structure and found to be effective there also.

### c. $N^+P$ Structure

Because of the problems with the  $NP^+P$  structure the simpler  $N^+P$  structure was also fabricated. This structure utilizes a deeply graded guardring to prevent edge breakdown. The guardring has a breakdown voltage larger than that of the avalanche region because of the large radius of curvature of the junction edge, and also because the junction is graded and depletes on either side of the junction. A cross-section of the structure is shown in Figure 5. Not shown in the figure is the  $P^+$ -inversion-stopper ring. The composite photomask layout for the structure is seen in Figure 6.

The diode was fabricated by doing planar diffusions into 6.5- $\Omega$ -cm P-type substrates. The N-type guardring diffusion is 5  $\mu$ m deep; the  $N^+$ -type active-region diffusion is approximately 1.0  $\mu$ m deep. The 6.5- $\Omega$ -cm substrate gives a 10- $\mu$ m depletion-layer width at an average breakdown voltage of 170 V.

Results of all runs were very good. No edge breakdown was observed. Premature microplasma breakdown resulting in low gain was observed on some diodes; however, the yield was very good. Gain of the good diodes was typically over  $10^3$  and uniform.

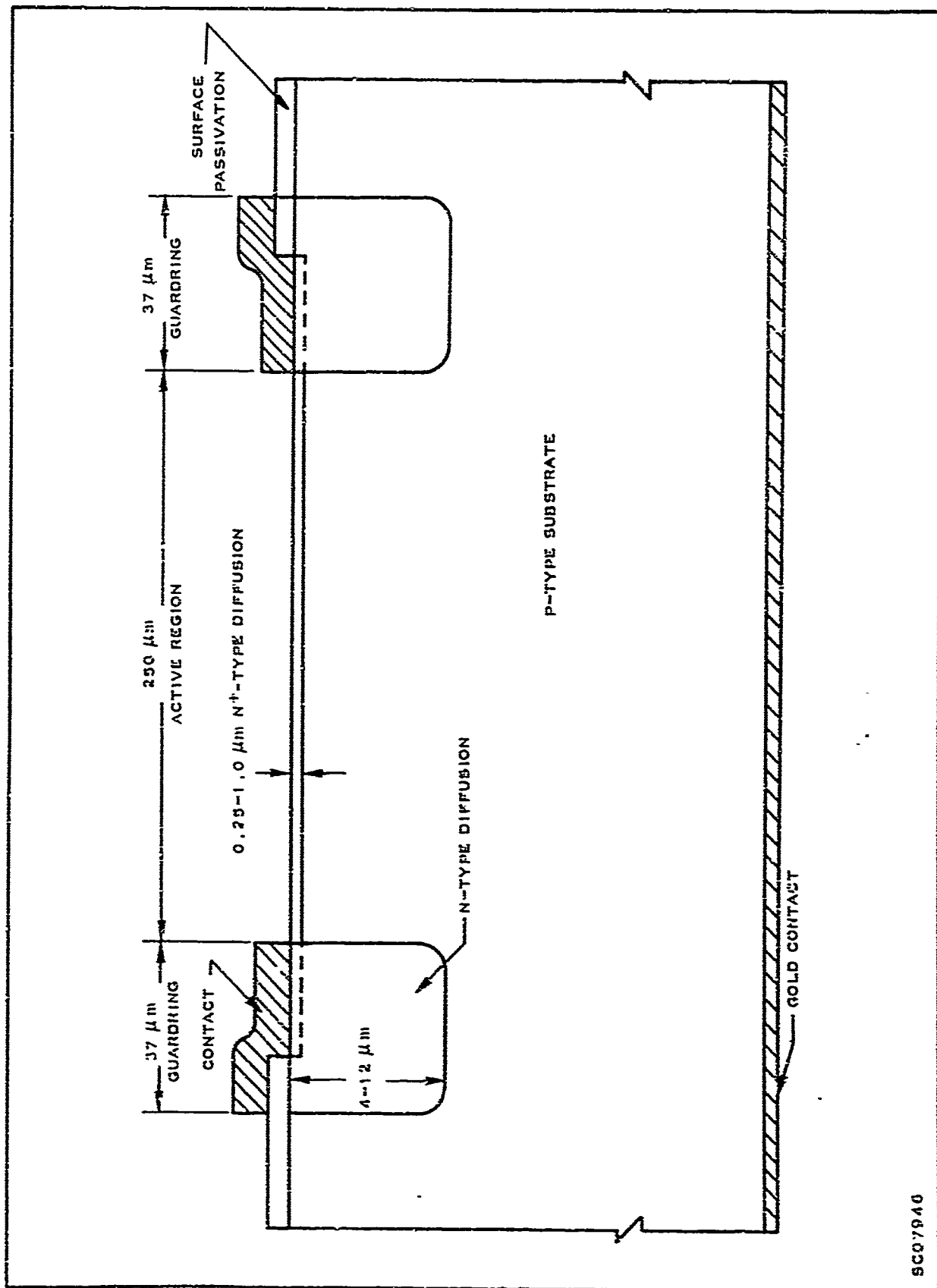


Figure 5. Graded-Guardring Avalanche Photodiode

SC07940

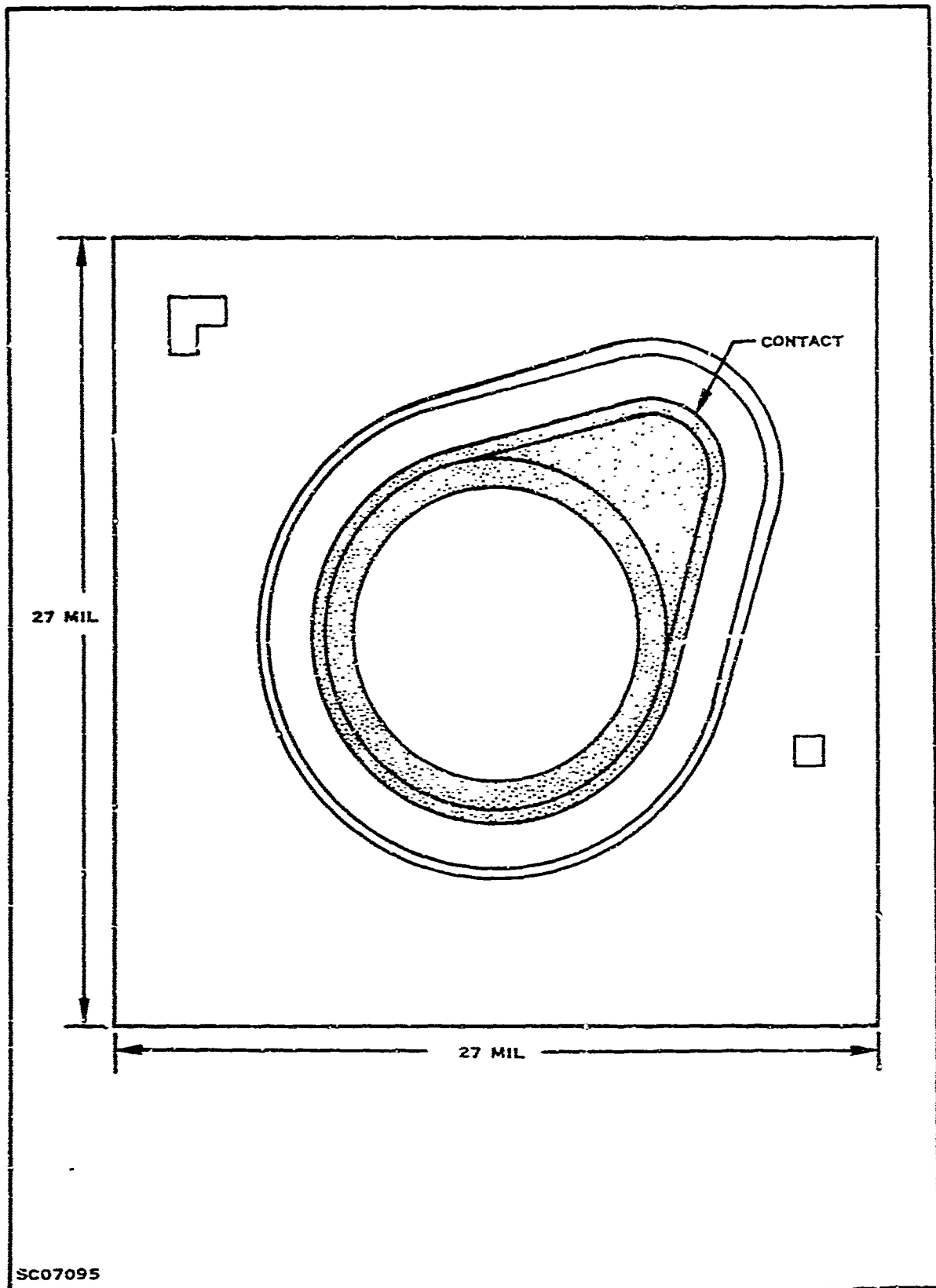


Figure 6. Composite Photomask Layout for Graded-Guardring Avalanche Photodiode

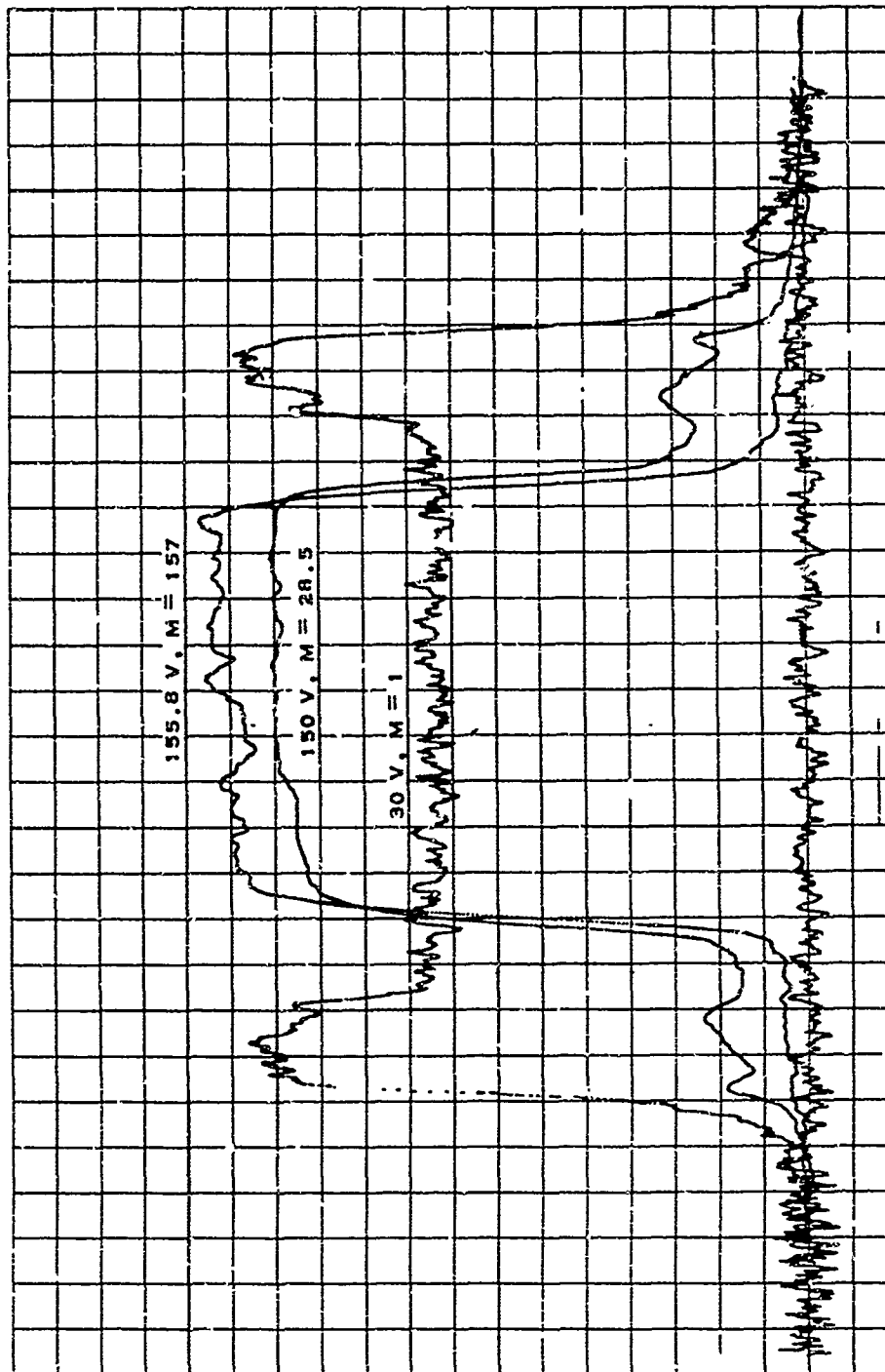
Optical-microprobe traces across the surface of a typical diode for several values of gain are shown in Figure 7. Traces were made before contacts were applied; therefore photoresponse is recorded across the entire diffused area for the trace  $M = 1$ . Also, the photoresponse indicated presence of an inversion layer cut to the inversion-stopper ring.

The amplifier gain was so reduced that the traces for  $M = 28.5$  and  $M = 157$  would be on scale. At a gain of 157 some variation of gain across the surface is observed; however, the variation is within  $\pm 5$  percent. The variation in the trace at a gain of one is due to noise in the amplifier. The other two traces clearly illustrate the improvement in signal-to-noise ratio obtained with avalanche gain.

At the end of the second quarter 10 each of the  $NP^+P$  and  $N^+P$  diodes were delivered under the contract. At the end of the fourth quarter 20 additional  $N^+P$  diodes were delivered, and a complete characterization of these diodes is given in the next section.

#### d. Package and Diode Mount

Ten of the 20 final diodes supplied on the contract were mounted in the coaxial pill package shown in Figure 8. Not seen is the lid, which has a lens formed in a 40-mil aperture. Using a collimated light source, such as a laser, the lens projects a spot on the diode less than 10 mils in diameter. The package can be mounted in a PC board or in a BNC connector, using the diode mount shown in Figure 9. With the diode and pin installed, the shell is slid inside the BNC connector, making sure the shell contacts the top ring of the diode. In the normal reverse-biased mode for the  $N^+P$  structure the pin is biased negative with respect to the shell. The other 10 diodes were mounted in a TO-18 package as shown in Figure 10.



SC07947

Figure 7. Photoresponse Across Surface of Graded-Guardring Structure

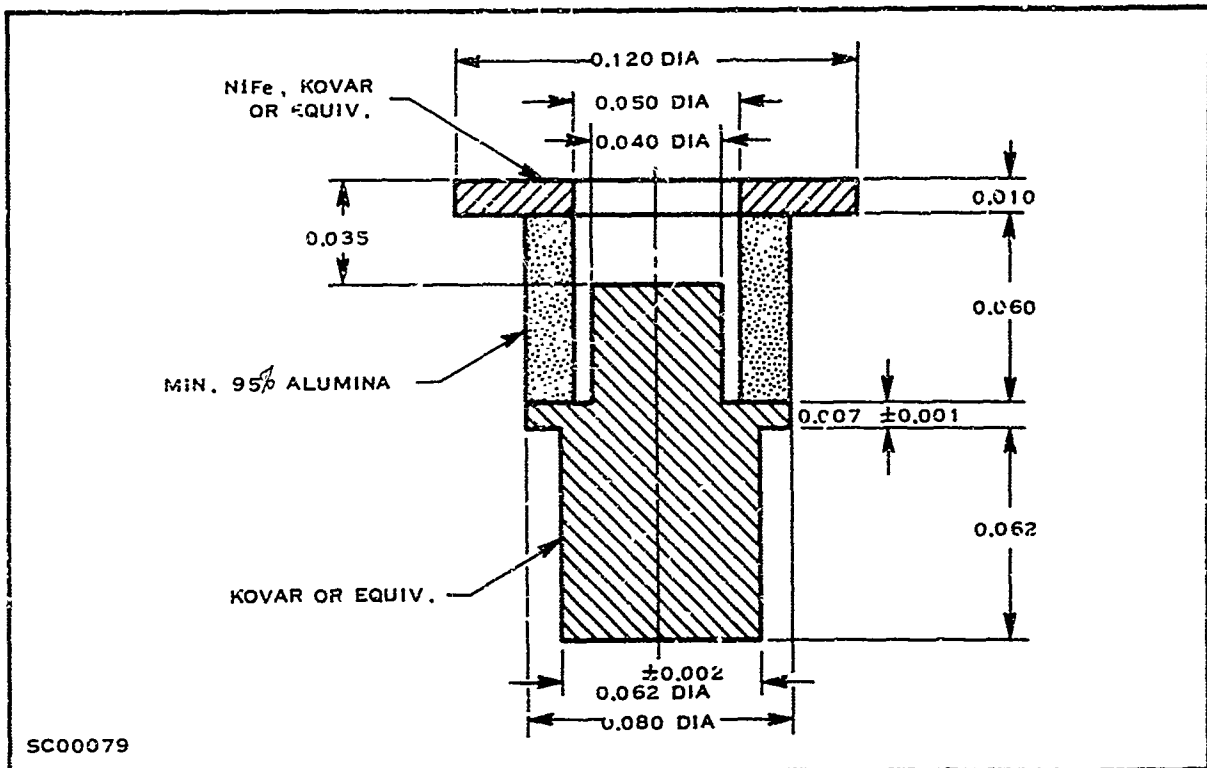


Figure 8. Coaxial Pill Package

## 2. Device Characterization

In this section the testing of the 20  $N^+P$  diodes is described, and the results are related to the expected theoretical performance. A summary of the diodes' characteristics is presented in the table on page 20.

### a. Gain Characteristics

Avalanche gain for the measurements was found by taking the ratio of the diode photocurrent at high reverse bias near breakdown to the photocurrent at a low bias voltage. The low-frequency measuring circuit is seen in Figure 11. The measurement was made using a 0.9- $\mu$ m gallium arsenide light-emitting diode modulated at 400 Hz. Using the photoresponse at 40 volts bias for a reference gain of one, the typical gain-voltage characteristic for a graded-guardring diode is shown in Figure 12.



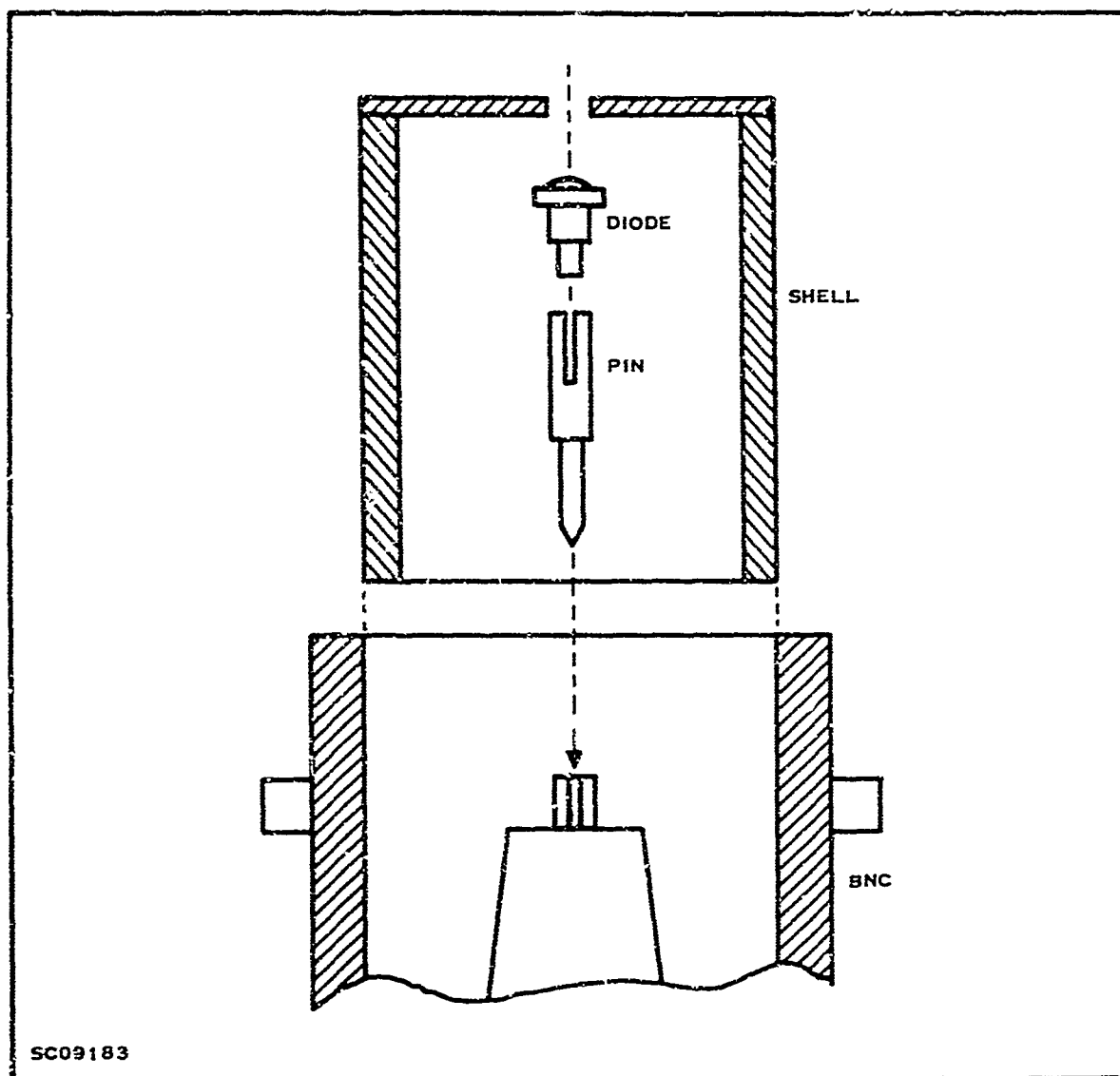


Figure 9. BNC Diode Mount

The gain-voltage characteristic for avalanche has been described by Miller <sup>4/</sup> as

$$M = \frac{1}{1 - (V/V_B)^n} \quad (1)$$

where

$V$  = diode voltage  
 $V_B$  = breakdown voltage  
 $n$  = empirical constant

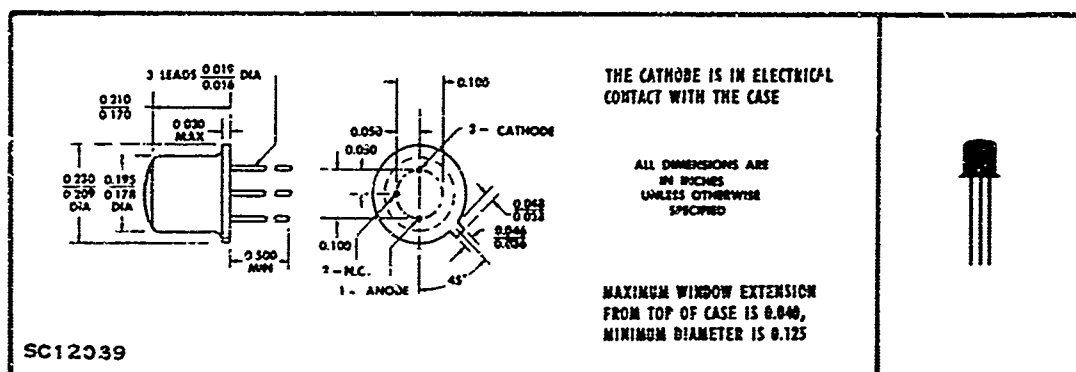


Figure 10. TO-18 Package

By plotting  $1/M$  versus  $V$  as shown in Figure 13, the breakdown voltage can be accurately determined. Breakdown voltage is defined as the voltage at which the avalanche gain approaches infinity or  $1/M$  approaches zero. By expanding the data of Figure 13 around 170 volts the breakdown voltage was found to be 170.26 volts. Using this value for  $V_B$  and the data given in Figure 12 the exponent,  $n$ , of Equation (1) can be determined. A plot of  $n$  versus  $V$  in Figure 14 shows that  $n$  is not constant for low gains. However, for gains greater than 62, the normal operating range,  $n$  is a constant, 0.3.

The breakdown voltage and gain discussed in the preceding paragraph are room-temperature values; however, since the impact ionization rates vary with temperature, there is a change in the breakdown voltage and a corresponding change in the gain with temperature. The breakdown voltage at 10  $\mu A$  dark current was measured on a group of diodes at temperatures from  $-50^\circ C$  to  $+50^\circ C$ . A plot of the typical diode characteristics is shown in Figure 15. The breakdown voltage increases with temperature at a rate of 194 mV/ $^\circ C$ . Other diodes having a higher breakdown voltage had a slightly higher slope, and vice versa. The temperature coefficient,  $\beta$ , of the breakdown voltage is often used when discussing a reference diode.

$$\beta = \frac{1}{V_B} \frac{dV_B}{dT} \quad (2)$$

For the diodes tested  $\beta$  was a constant,  $1.15 \times 10^{-3}/1^\circ C$ .

## Summary of Diode Characteristics

Diode No.	Package	V at M=160 Volts	M <sub>T</sub>	d	I <sub>CO</sub> (nA)	I <sub>S</sub> (nA)
11	P111	173.49	620	2.58	0.56	7
12	P111	160.93	200	2.52	0.97	8
13	P111	171.71	400	2.48	0.615	23
14	P111	171.35	400	2.48	0.51	23
15	P111	169.72	> 1000	2.50	0.276	12
16	P111	170.42	400	2.54	0.22	6
17	P111	165.84	> 1000	2.51	0.915	10
18	P111	164.68	160	2.53	0.077	2.2
19	P111	168.85	620	2.56	0.454	3
20	P111	161.47	400	2.52	0.23	4
21	TO-18	160.82	> 1000	2.54	0.85	25
22	TO-18	169.15	> 1000	2.54	0.62	8
23	TO-18	165.75	250	2.58	0.66	17
24	TO-18	167.95	> 1000	2.57	0.34	3.5
25	TO-18	159.77	> 1000	2.59	1.24	14
26	TO-18	164.74	> 1000	2.54	0.83	25
27	TO-18	153.82	400	2.54	0.87	30
28	TO-18	167.59	> 1000	2.58	0.36	5.5
29	TO-18	172.38	> 1000	2.54	0.56	10
30	TO-18	168.62	> 1000	7.53	0.61	9.5

As the avalanche gain is a sensitive function of the ratio  $V/V_B$ , and since  $V_B$  changes with temperature, maintaining a constant responsivity in the detector could be a problem. This problem has been overcome by using an automatic bias circuit, as shown in Figure 16. <sup>5/</sup> This circuit uses another photodiode as a reference diode. The reference diode senses any changes in temperature, and controls the series regulator transistor,  $Q_3$ , through the feedback amplifier  $Q_1$  and  $Q_2$ . If the reference diode has the

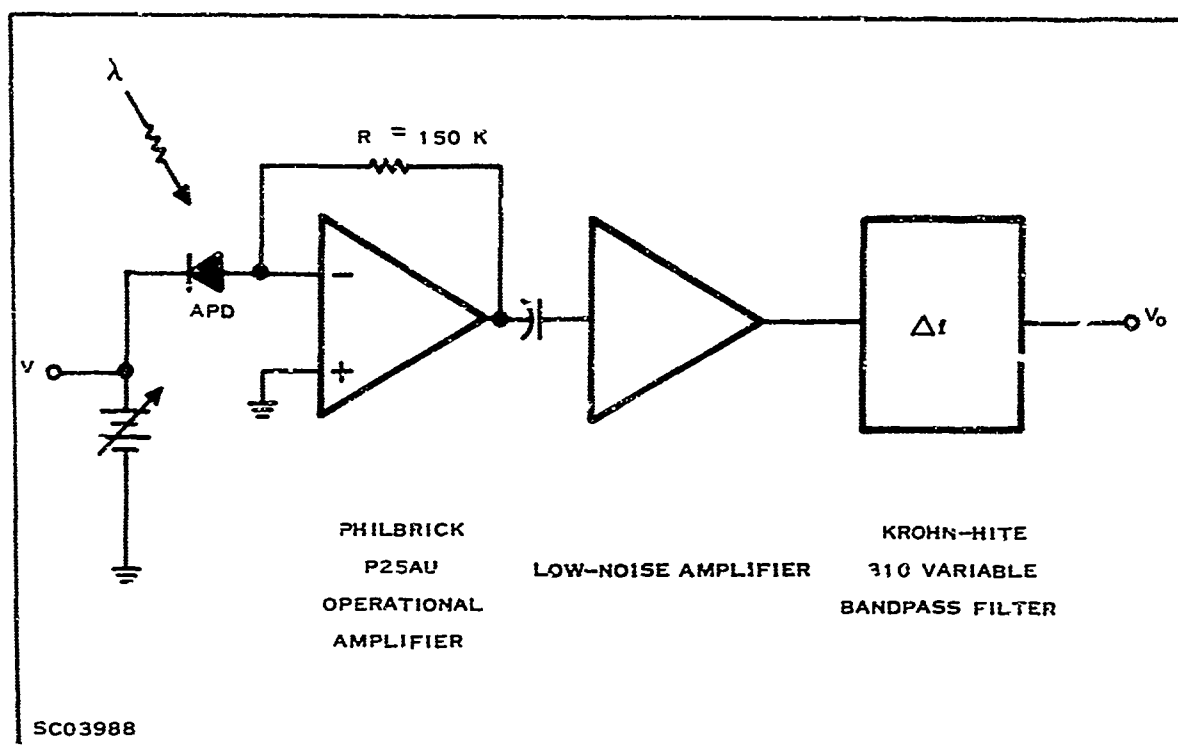


Figure 11. Low-Frequency Gain and Noise Measurement Circuit

same breakdown voltage and temperature coefficient as the photodiode, then the gain of the photodiode is constant.

$$M = \frac{1}{\frac{K V_B}{1 - \left(\frac{K V_B}{V_B}\right)^n}}$$

$$M = \frac{1}{1 - K^n} \quad (3)$$

K is the output voltage ratio of  $R_3$ . The photon-coupled transistor,  $Q_3$ , uses a gallium arsenide light-emitting diode for dc isolation of the input voltage and the feedback amplifier, thus allowing a single bias circuit to be used for a wide range of breakdown voltages.

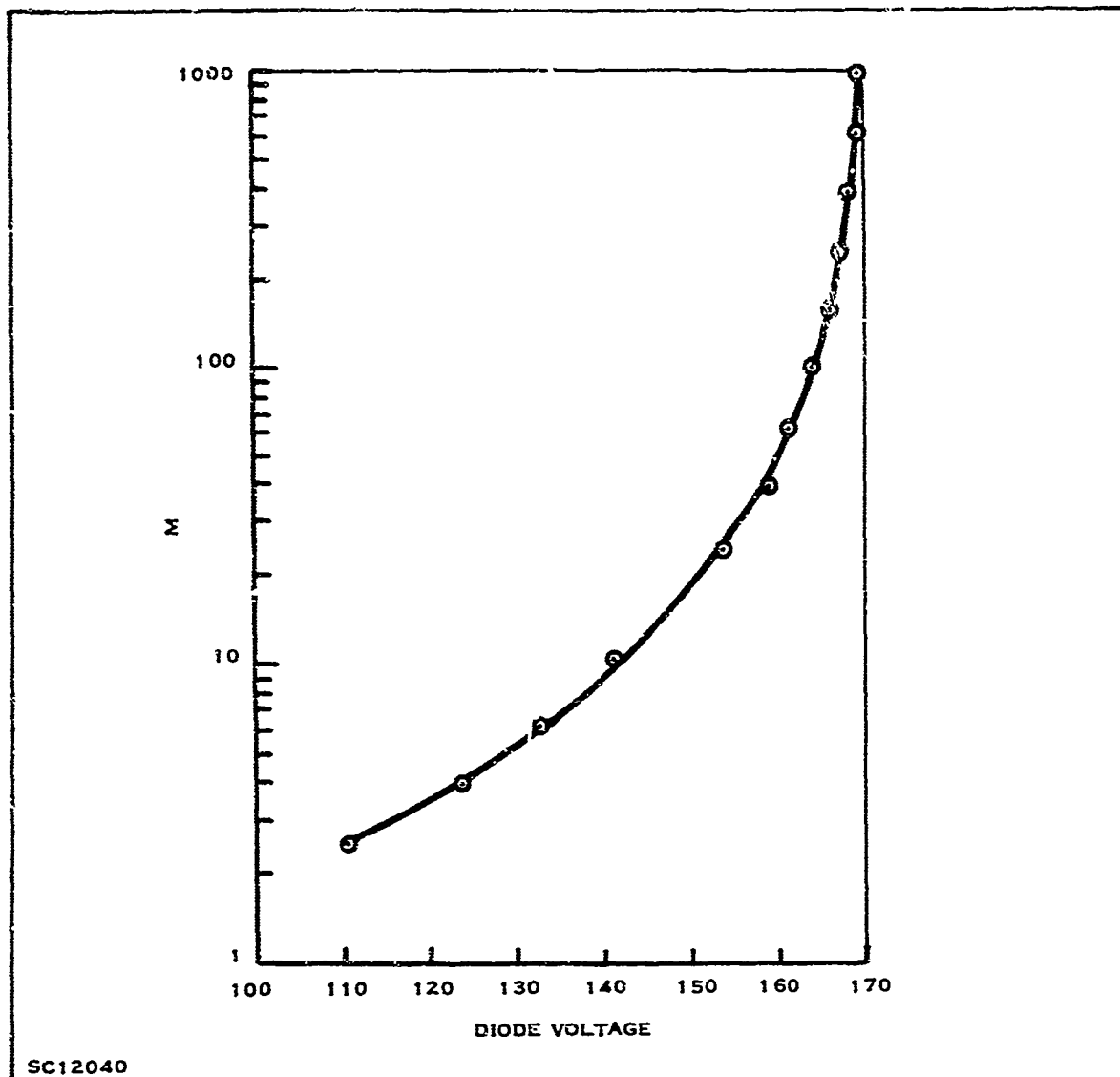
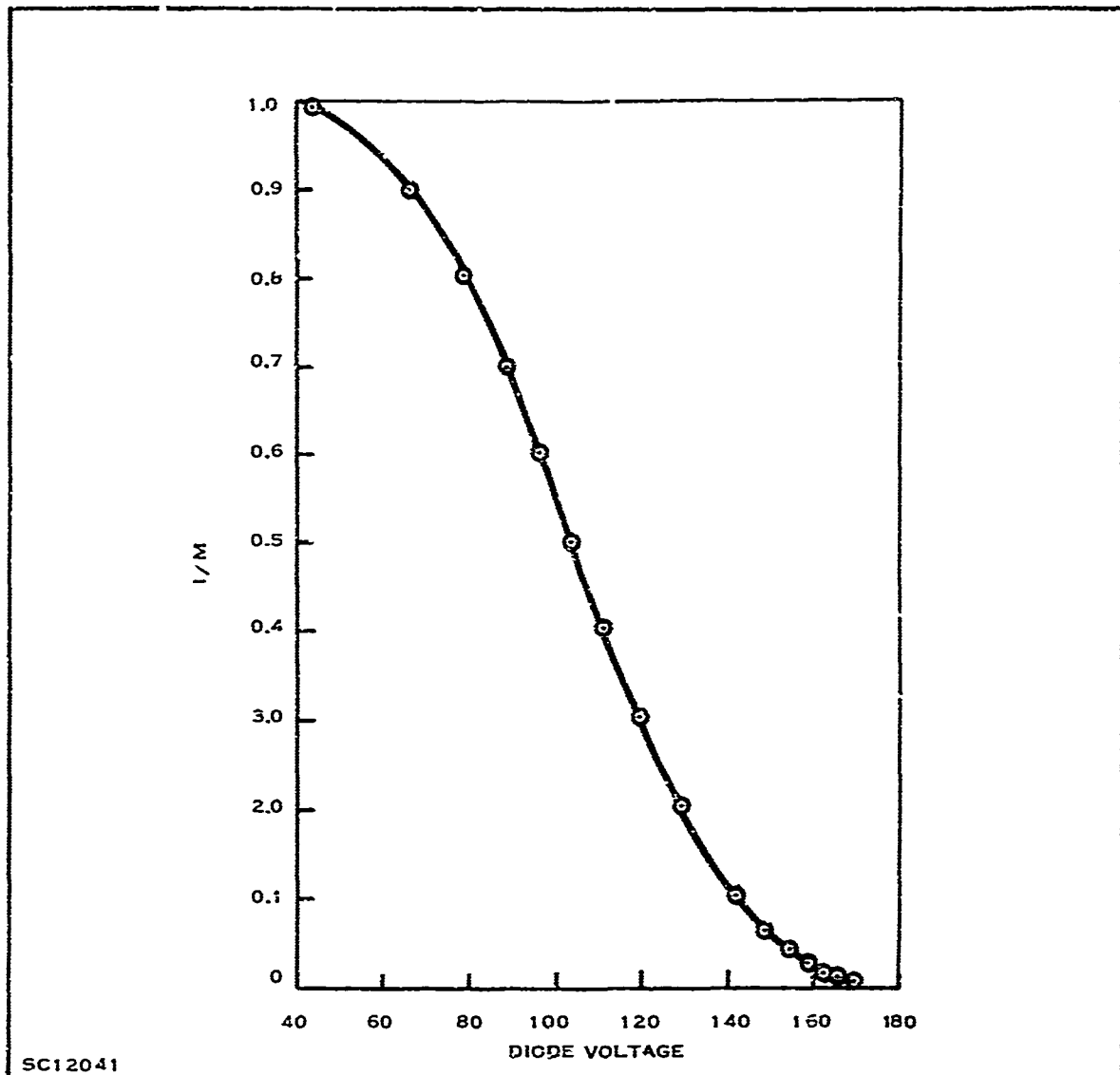


Figure 12. Avalanche Gain versus Bias Voltage for Typical N<sup>+</sup>P Diode at 0.9 μm

b. Quantum Efficiency

The quantum efficiency,  $\eta$ , of a photodiode is defined as the ratio of the total photocurrent collected at the junction,  $I_{\phi}$ , to the photon current incident on the surface of the photodiode,  $q\phi_0$

$$\eta = \frac{I_{\phi}}{q\phi_0} \quad (4)$$

Figure 13. I/M versus Voltage at 0.9  $\mu\text{m}$ 

If light is allowed to enter the detector only from the top and within the active area, then  $\eta$  is based on Lambert's law

$$\phi(x) = \phi_0 (1 - R) e^{-\alpha x} \quad (5)$$

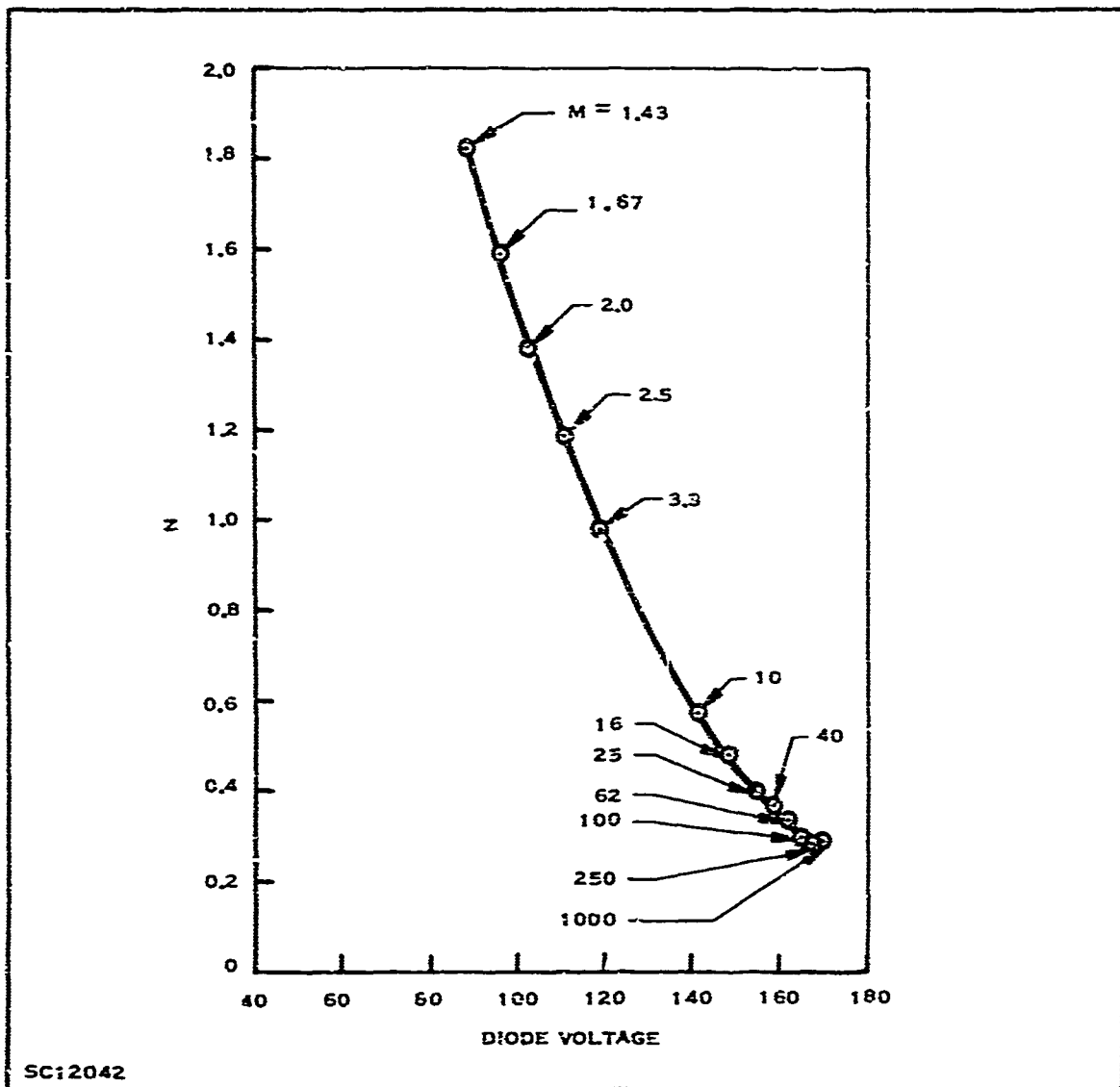
where

$\phi(x)$  = photon flux at  $x$

$x$  = distance below surface

$R$  = reflection at the surface

$\alpha$  = absorption coefficient for detector material and wavelength light.

Figure 14.  $\eta$  versus Voltage at  $0.9 \mu\text{m}$ 

In a silicon avalanche photodetector the quantum efficiency is complicated by the fact that electrons have an impact ionization rate much higher than that for holes; therefore only electrons initiate avalanche multiplication. In the structure shown in Figure 1 only light absorbed below the junction generates carriers which are multiplied; the hole is the carrier which moves to the avalanching junction in the N-type diffuse area. The total quantum efficiency is composed of the electron quantum efficiency,

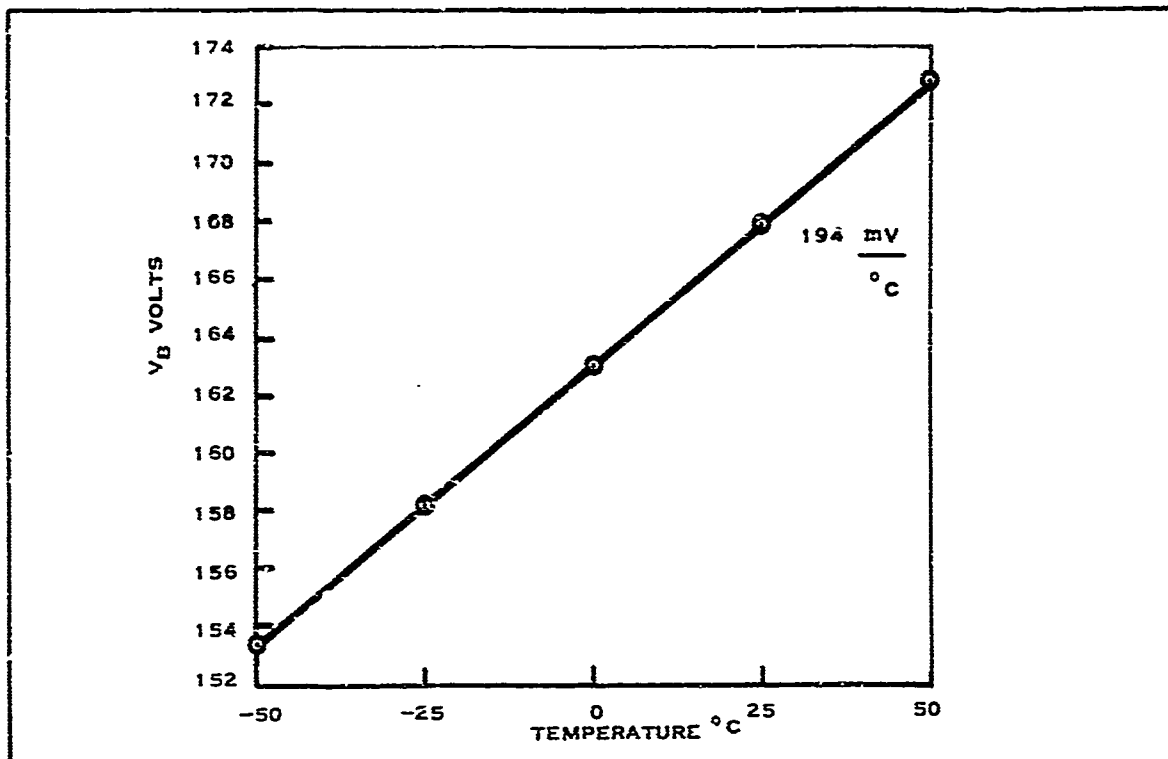


Figure 15. Breakdown Voltage versus Temperature

$\eta_n$ , and the hole quantum efficiency,  $\eta_p$ ; however, only  $\eta_n$  contributes to signal at high avalanche gains.

$$\eta = \eta_n + \eta_p \quad (6)$$

For a given junction depth the maximum value for  $\eta_n$  is

$$\eta = \eta_{n(\max)} = e^{-\alpha x_j} \quad (7)$$

It could be lower if some of the light were absorbed below the depletion depth and the carriers were recombined before they reached the junction.

Spectral response measurements were made on several of the diodes, using a Perkin-Elmer spectrometer, a tungsten lamp,



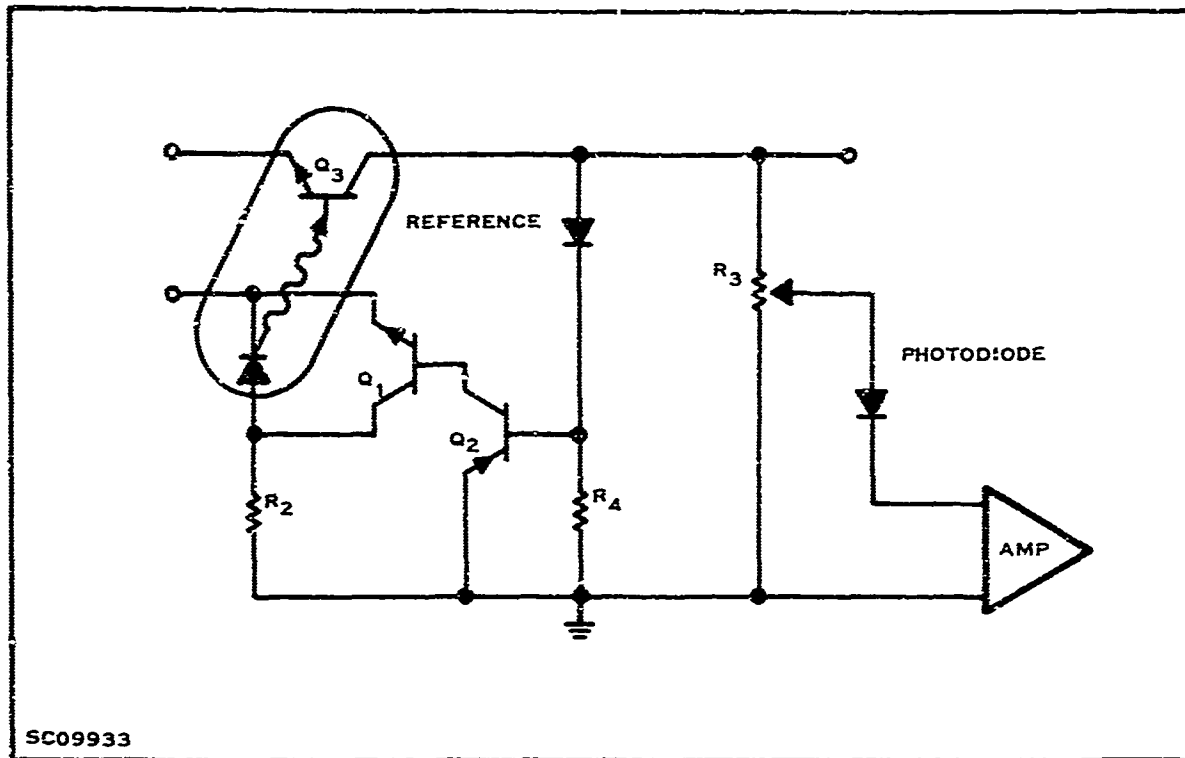


Figure 16. Automatic Bias Circuit

and a thermocouple as a flat power detector. Knowing the photon energy, we converted the data to a relative quantum efficiency. Measurements were made at a high avalanche gain so that only  $\eta_n$  was measured. The results for an antireflection coated diode and an uncoated diode are shown in Figure 17. Diodes supplied in the pill package received a  $\lambda/4$  at  $0.9 \mu\text{m}$  coating of  $\text{SiO}_2$  to reduce the surface reflection. Coating resulted in approximately 45 percent improvement in quantum efficiency at  $0.9 \mu\text{m}$ . Diodes supplied in the TO-18 package were not coated.

In the model of an avalanche photodiode it is best to use the actual electron gain instead of apparent or measured gain. There can be a difference because of the differences in electron and hole quantum efficiencies. The measured gain as defined earlier can be written in terms of the electron and hole gains and quantum efficiencies as:

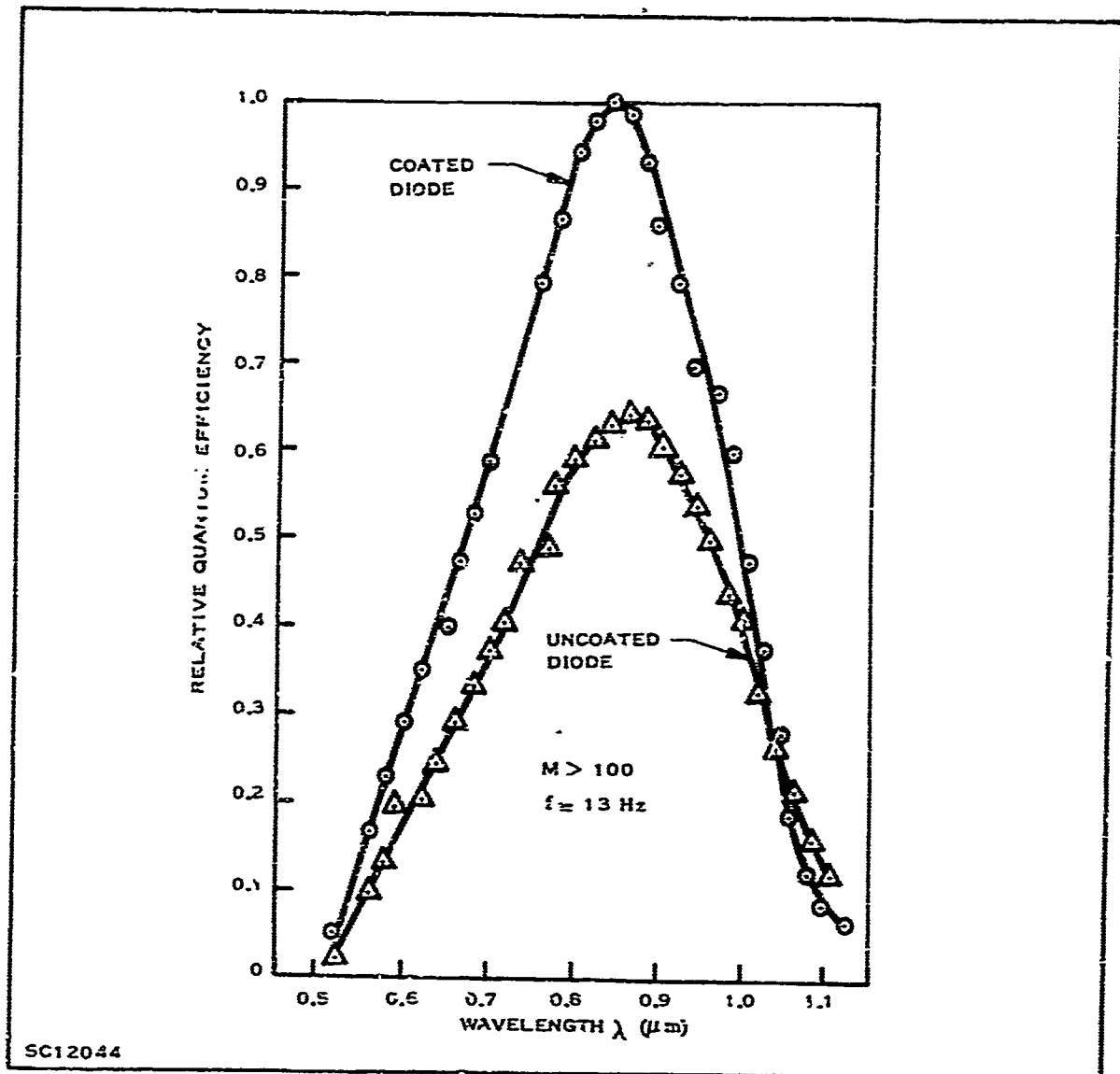


Figure 17. Typical Electron Quantum Efficiency for  $N^+P$  Diode

$$M = \frac{\eta_p M_p + \eta_n M_n}{\eta_p + \eta_n} \quad (8)$$

where

$M$  = measured gain  
 $M_p$  = hole gain ( $\approx 1$ )  
 $M_n$  = electron gain.

At high electron gains Equation (8) can be written

$$\frac{M}{M_n} = \frac{\eta_n}{\eta_D + \eta_n} \quad (9')$$

For  $\lambda = 0.9 \mu\text{m}$ ,  $\eta_p$  is small and the measured gain is essentially equal to the electron gain. A plot of the measured gain at  $0.6328 \mu\text{m}$  versus the  $0.9 \mu\text{m}$  gain is seen in Figure 18. The gains were measured at the same reverse bias voltages. If it is assumed that the total quantum efficiency at  $0.6328 \mu\text{m}$  is 100 percent then the junction depth can be calculated from the slope of the curve, Equation (9), and Equation (7).

$$\eta_n = \frac{M}{M_n} = 0.38$$

$$\alpha = 3.7 \times 10^3 \text{ (Dash and Newman } \frac{6}{1} \text{)}$$

$$\eta_n = e^{-3.7 \times 10^3 x_j}$$

$$x_j = 2.6 \mu\text{m}$$

This represents a minimum junction depth, since  $\eta$  was assumed to be 1.0. Although this large junction depth was not expected, the low electron quantum efficiency at  $0.6328 \mu\text{m}$  from Figure 17 supports the results of the calculations above.

One explanation for the low quantum efficiency and apparently deep junction is that the absorption coefficient is actually larger than the value used in the calculation.

One additional aspect of the quantum efficiency concerns the frequency response. The quantum efficiency in the discussion above has been the low frequency or dc quantum efficiency. Carriers which are generated outside the depletion region reach the junction by diffusion, a relatively slow process. At  $0.9 \mu\text{m}$  the light has a large penetration depth ( $\alpha = 5 \times 10^2 \text{ cm}^{-1}$ ). For

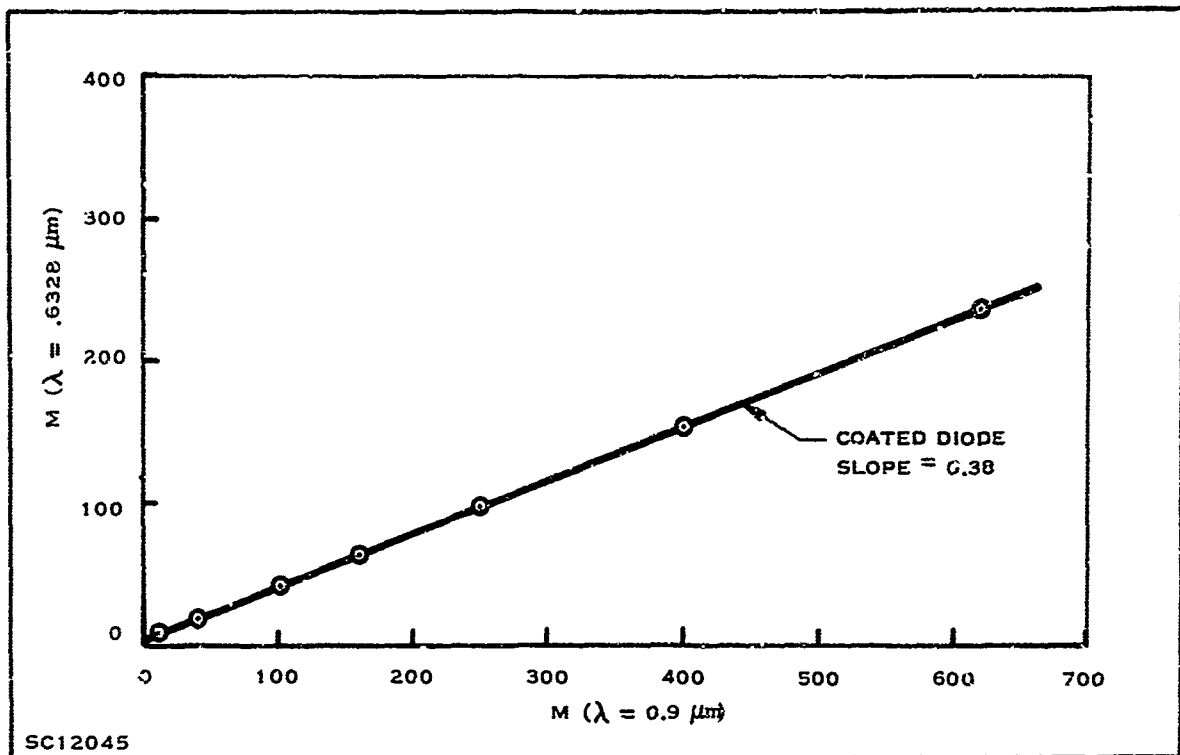


Figure 18. Gain at 0.9  $\mu\text{m}$  versus Gain at 0.6328  $\mu\text{m}$

this reason it is difficult to obtain a silicon avalanche photodiode with a high ac quantum efficiency. For the structure shown in Figure 1 the high-frequency electron quantum efficiency,  $\eta_a$ , can be written

$$\eta_a = e^{-x_j} - e^{-x_d} \quad (10)$$

With a depletion width of 10  $\mu\text{m}$  and  $x_j = 2.6 \mu\text{m}$ ,  $\eta_a$  would be approximately 35 percent.

The quantum efficiency versus modulation frequency was measured using a 0.9  $\mu\text{m}$  gallium arsenide light-emitting diode. A germanium photodiode was employed to calibrate the light source. Results are shown in Figure 19. At 60 kHz the response begins to fall off, dropping to a value of approximately 40 percent at 40 MHz. If we normalize the data to  $\eta_n = 88$  percent at 0.9  $\mu\text{m}$  (Figure 17) then the measured  $\eta_a$  is approximately 35 percent, the

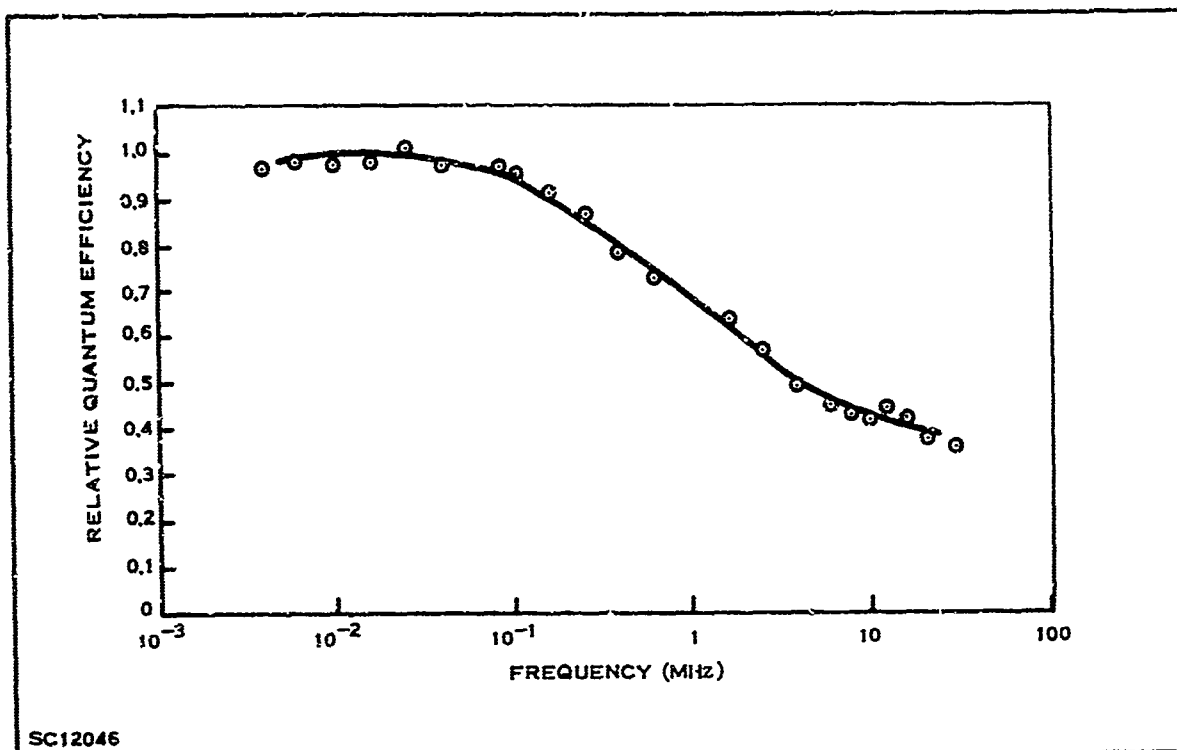


Figure 19. Frequency Response of Quantum Efficiency

same as that calculated from Equation (10). If the depletion width were doubled, then Equation (10) shows that  $\eta_a$  would be increased to 56 percent; however, this would require a breakdown voltage of approximately 350 volts.

### c. Leakage Currents

Leakage current in an avalanche photodiode consists of the unmultiplied surface leakage and the multiplied bulk leakage,

$$I_L = I_S + MI_{co} \quad (11)$$

where

- $I_L$  = total dark leakage current
- $I_S$  = unmultiplied surface leakage
- $I_{co}$  = multiplied bulk leakage.

Avalanche gains allow the two components to be determined, as seen in Figure 20. The total measured dark leakage is plotted versus the electron gain ( $M$  at  $0.9 \mu\text{m}$ ). The slope of the line is  $I_{\text{co}}$ , and the current intercept is the surface leakage. The results,  $I_{\text{co}} = 0.28 \text{ nA}$  and  $I_{\text{S}} = 12 \text{ nA}$ , are typical for the diodes.

In silicon the bulk leakage current is due mainly to thermally generated carriers in the depletion region, instead of the diffusion currents as in germanium. The carriers, thermally generated, are swept to the junction before recombination can occur. The current then is a function of the volume of the depletion region, and the lifetime  $\tau$

$$I_{\text{co}} = \frac{q W_{\text{d}} n_{\text{i}} A}{2\tau_0} \quad (12)$$

where

- $q$  = electron charge
- $W_{\text{d}}$  = depletion layer width
- $n_{\text{i}}$  = intrinsic carrier density
- $\tau_0$  = carrier lifetime
- $A$  = area of active region.

For diode No. 15, shown in Figure 20, the lifetime of the bulk material is  $3.9 \mu\text{s}$ . Diode No. 18 had the lowest bulk leakage,  $0.077 \text{ nA}$ , which would indicate a bulk lifetime of  $14.3 \mu\text{s}$ . Calculating the diffusion length,  $L$ , from

$$L = \sqrt{D\tau_0} \quad (13)$$

where  $D$  = electron diffusion constant, the respective diffusion lengths are  $110 \mu\text{m}$  and  $210 \mu\text{m}$ . These lifetimes and diffusion lengths are very good for finished silicon devices, indicating that the low leakage currents are in line with the state of the art.

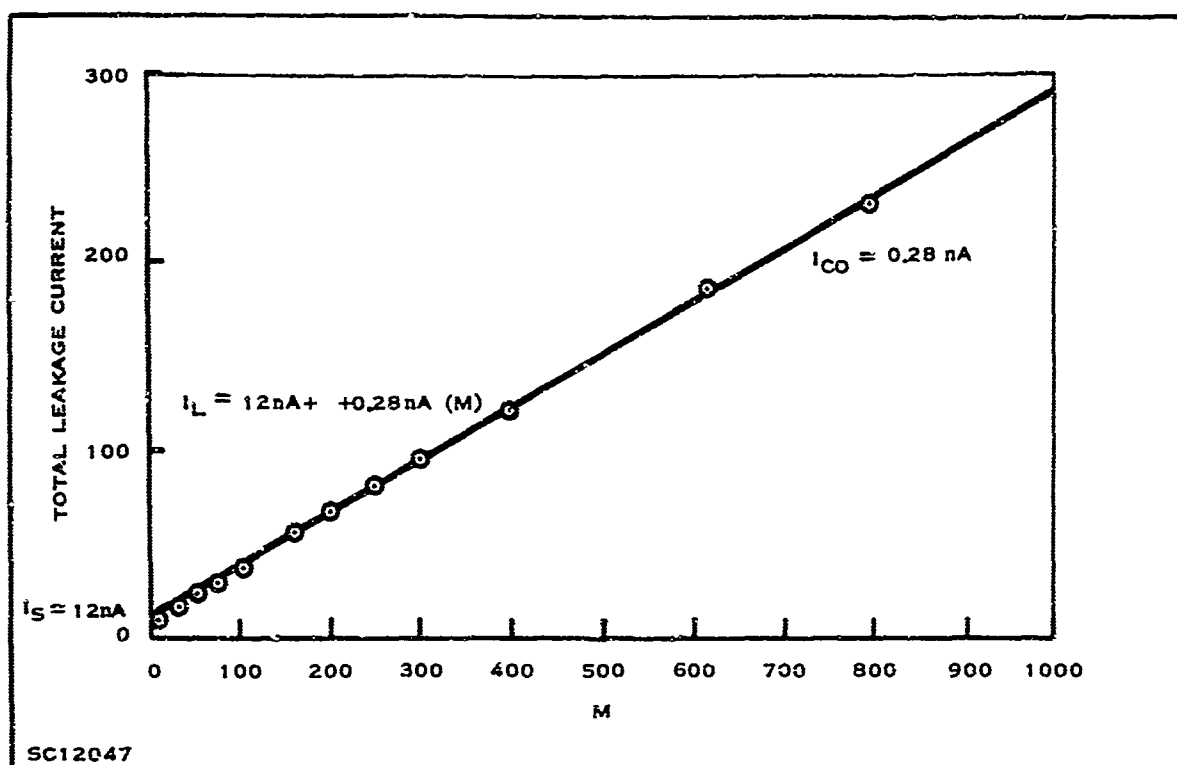


Figure 20. Total Leakage Current versus Gain

#### d. Avalanche Noise

Because of the statistical nature of avalanche multiplication the noise power is found to increase at a faster rate with gain than does the signal power. The noise of the avalanche process has been described by McIntyre <sup>3/</sup> as

$$i_n^2 = 2q \Delta f I M^d \quad (14)$$

where

$\Delta f$  = noise bandwidth

$I$  = dc current that is multiplied

$d$  = constant dependent on electron and hole ionization rates.

Avalanche noise versus gain at 0.9  $\mu\text{m}$  was measured on each of the 20 diodes. The noise bandwidth of the system was 2.3 kHz at a center frequency of 3.8 kHz. The noise was produced by the sum of the bulk leakage current,  $I_{CO}$ , and the collected photocurrent,  $I_\phi$ . Typical values for  $I$  ranged from 2 to 5 nA. The system has

an ac current to voltage transimpedance of  $1.05 \times 10^9$  ohms. System noise at the output was 37 mV. A block diagram of the noise-measurement circuit is seen in Figure 11.

A typical plot of output noise versus gain is shown in Figure 21. Equation (14) predicts a straight-line relationship as seen in this figure. Deviation of the measured values from this at low gains is due to the system noise. The point at  $M = 1$  was calculated from Equation (14) and the system transimpedance. The slope of the straight line has a value of  $d/2$  indicating that  $d$  is 2.58 for the diode. That value is typical for this series of measurements, and we do not understand why it is higher than the values obtained during the third quarter on identical diodes.

Deviation from the straight line is due to micro-plasma breakdown and occurs at  $M_T$ , defined as the gain of first sustained breakdown. Range of  $M_T$  for the diodes was from 160 to greater than  $10^3$ .

#### e. Equivalent Circuit

The avalanche photodiode can be represented by the equivalent circuit seen in Figure 22. This is essentially the same circuit as given by Melchoir and Lynch,<sup>9/</sup> except for an admittance in parallel with the current source. The admittance, consisting of a series resistor and inductor, is not seen in Figure 22, since in silicon the current levels are low and the resistance is normally high. The inductance includes gain-bandwidth limitations which will be discussed later.

The signal current source,  $i_s$ , can be represented by

$$i_s = q \phi(t) \eta_a M_n \quad (15)$$



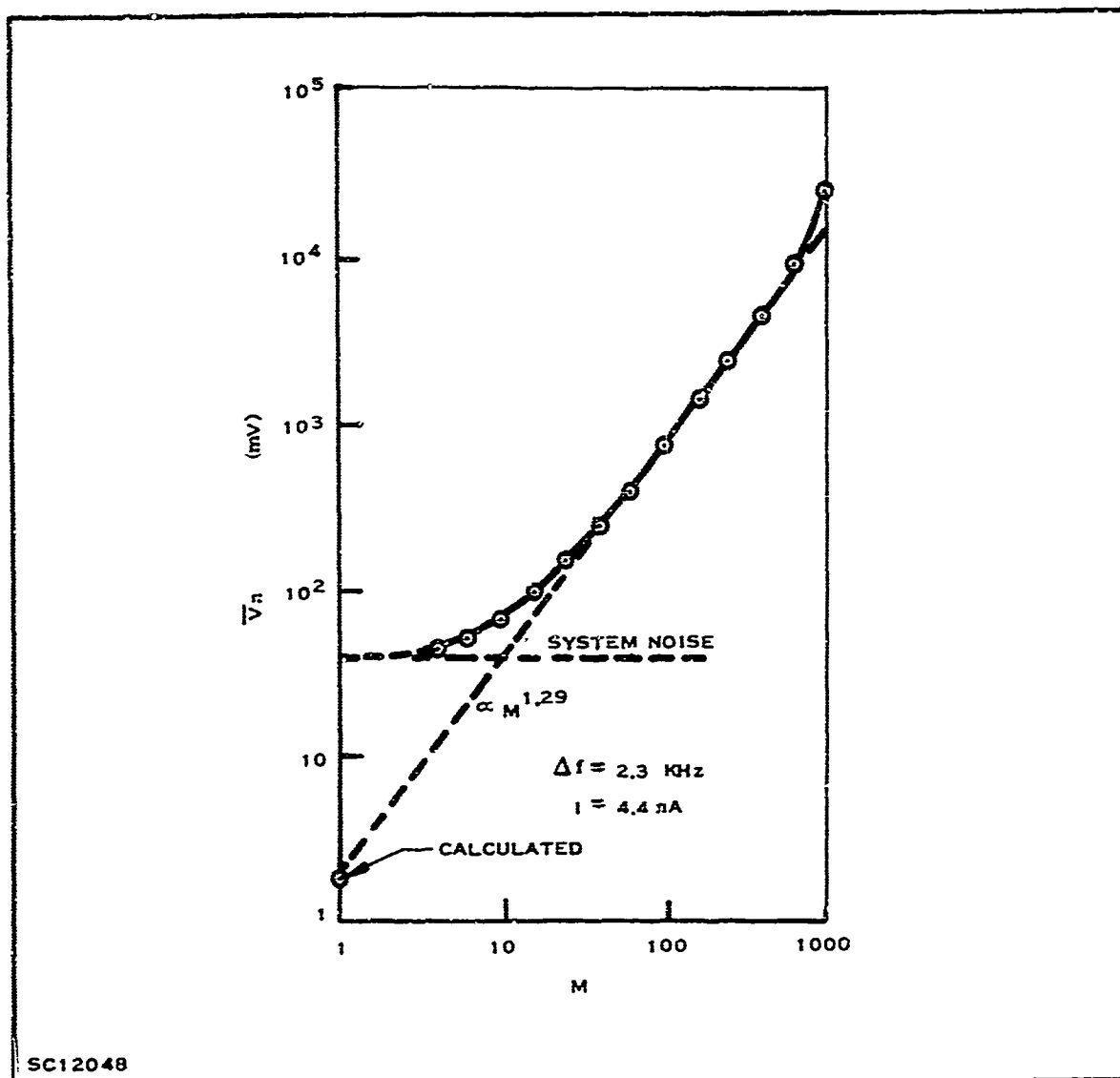


Figure 21. Avalanche Noise Voltage versus Gain

where  $\phi(t)$  is the modulated optical carrier. In parallel with the signal current source is the avalanche noise source. Space charge layer resistance,  $R_c$ , is included to describe the lowering of the electric field due to widening of the depletion layer.<sup>10/</sup> For the  $N^+P$  structure

$$R_c = \frac{W_d^2}{n_e A v_s} \quad (16)$$

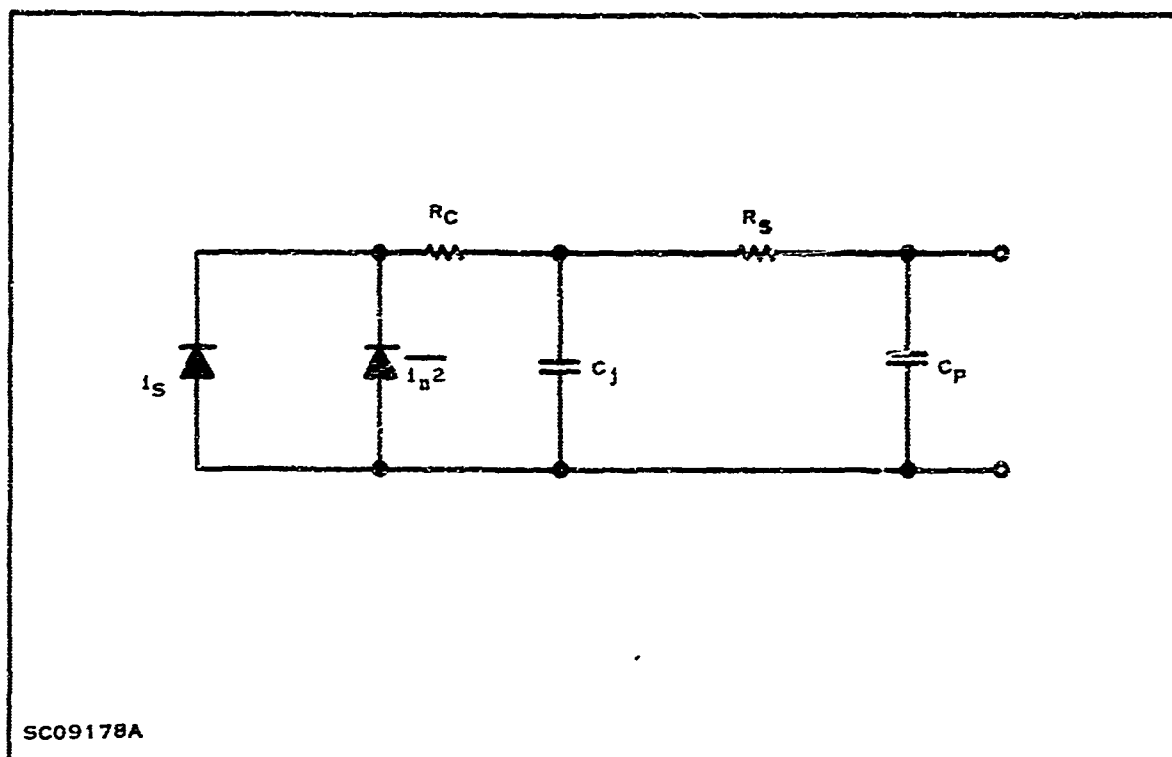


Figure 22. Avalanche Photodiode Equivalent Circuit

where  $v_s$  = hole-saturated drift velocity. Calculations show  $R_C$  to be approximately 100 ohms.

The junction capacitance,  $C_j$ , and pill-package capacitance were measured at 1.0 MHz and found to be 1.3 pF and 0.25 pF respectively at high gains.

Measurements made on the diodes at 900 MHz, using a GR-1602 UHF admittance meter, showed the diode series resistance  $R_S$  to be 50 ohms, and  $C_j$  and  $C_P$  to be 1.3 pF and 0.24 pF respectively.

#### f. Frequency Limitations

Other than the cutoff of the low-frequency quantum efficiency (Figure 19), three effects can limit the frequency response of an avalanche photodiode. First of these is the RC cutoff due to junction capacitance and series resistance. If the

diode is fed into a low-impedance amplifier then the RC cutoff due to  $R_s = 50$  ohm and  $C_j = 1.3$  pF is 2.4 GHz, or a rise time of 0.14 ns. This can be improved by conjugately matching the diode.

There is a frequency limitation due to the transit time of carriers moving across the depletion region. This transit time is given by

$$T = \frac{W_d}{V_s} \quad (17)$$

where  $V_s$  is the saturated drift velocity typically  $10^7$  cm/sec for electrons in silicon. The transit time cut-off frequency has been shown by Gartner<sup>11/</sup> to be

$$\omega_t = \frac{2.8}{T} \quad (18)$$

For the structure shown in Figure 1 the transit time cut-off frequency is 3.6 GHz.

The other frequency limitation is due to the multiple transits of carriers through the thin avalanche region, and the corresponding time for the avalanche multiplication to occur. This, normally represented as a gain-bandwidth product, has been treated in detail by Emmons.<sup>12/</sup>

The ac gain,  $M_{ac}$ , at 509 MHz was measured as a function of the dc gain,  $M_{dc}$ . The same measurement was made during the third quarter while holding  $M_{dc}$   $I_d$  constant at 1.0 mA to avoid current-saturation effects. When this was repeated, saturation was found to be present, and the new measurements were made at much lower dc currents. Only the 508-MHz laser beat was used because of the instability of the 1.0-GHz beat. The laser was operated at the 0.6328- $\mu$ m line. The lower signal levels required a more sensitive ac detector; a GR-DNT heterodyne detector was used. The input photocurrent was held constant; therefore the total unmultiplied current,  $I$ , was composed of the photocurrent plus the

bulk leakage current. The results for two values of  $I$  are shown in Figure 23. Even with the low currents there apparently is some current-dependent gain saturation. Probably this could be explained by the shunt admittance described by Melchoir and Lynch.<sup>9/</sup> Based on the maximum  $M_{ac}$  obtained for the two currents, the gain-bandwidth product is approximately 70 and 50 GHz.

Since the light used for the measurement was at  $0.6328 \mu\text{m}$  and the actual electron gain was higher by the factor  $1/0.38$  (Figure 18) then the gain-bandwidth products would be 190 GHz and 130 GHz respectively. Although these values are in the range expected, it is difficult to assign any degree of accuracy to the values. It is recommended that further work be done in the area of correlating experimental results with the theory.

g. NEP

The avalanche mechanism is used in a photodiode to achieve improved sensitivity in a photodetector system which normally would be limited by noise in the preamplifier. A convenient figure of merit in describing the noise performance of a detector system is the noise-equivalent power (NEP). The effect of avalanche gain on NEP has been discussed by Biard and Shaunfield.<sup>13/</sup> The NEP of a photodetector using the  $N^+P$  avalanche photodiodes was measured and compared with the theory.

By definition the NEP of a complete photodetector is the rms value of sinusoidally modulated radiant power falling on the detector, which gives rise to a signal-to-noise ratio of 1, referred to the detector terminals in a reference bandwidth of 1.0 Hz. The analysis shows that the NEP can be expressed with three terms.<sup>13/</sup>

$$\text{NEP} = \sqrt{A + A^2 + B^2 + C^2} \quad (19)$$

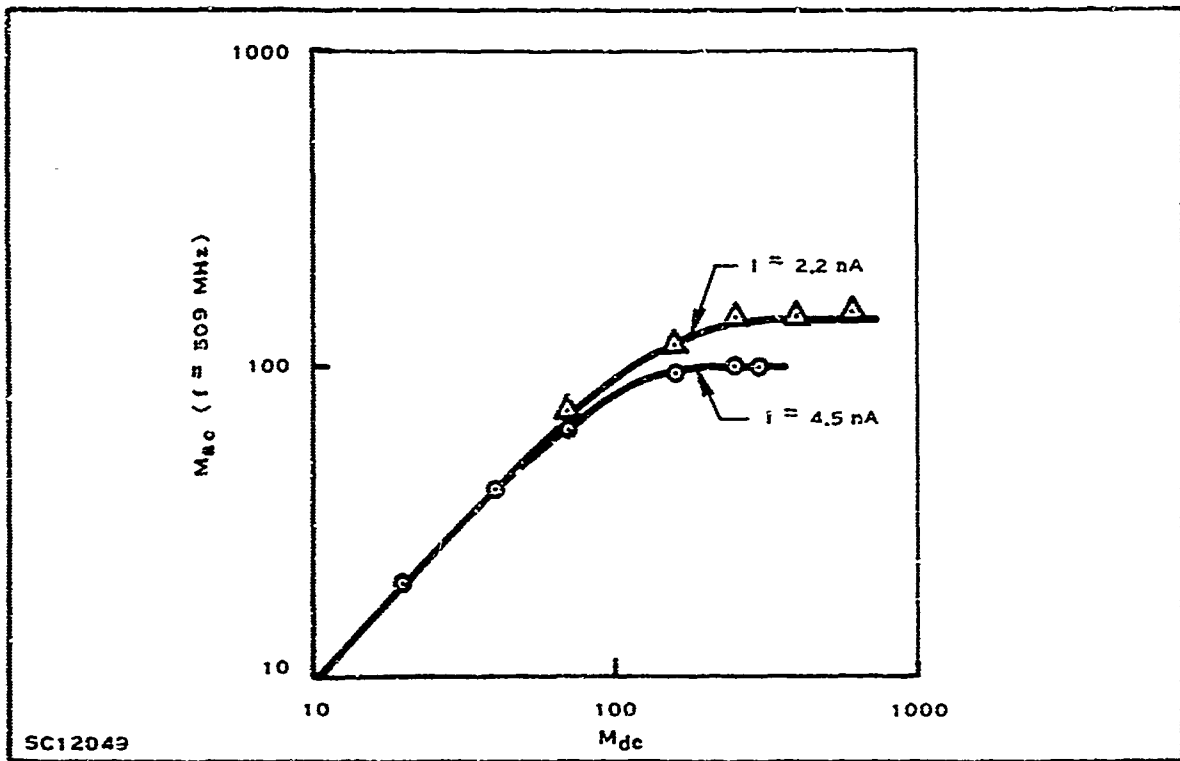


Figure 23. AC versus DC Gain

where

$$A = \frac{q E_p \eta_o \sqrt{2\Delta f}}{m \eta_a^2} \cdot M^{d-2} \quad (20)$$

$$B = \frac{E_p \sqrt{2q I_{CO}}}{\eta_a} \cdot M^{d-2} \quad (21)$$

$$C = \frac{E_p \sqrt{2q I_x}}{\eta_a} \cdot M^{-1} \quad (22)$$

$\eta_o$  = dc quantum efficiency

$\eta_a$  = ac quantum efficiency

$I_x$  = equivalent dc current which would produce shot noise at the input equal to the actual noise.

$I_{CO}$  = bulk leakage current

$E_p$  = photon energy

$m$  = modulation index

$\Delta f$  = noise bandwidth

$d$  = noise slope

$M$  = avalanche gain.

Term A is the NEP due to the shot noise on the dc component of the input signal. Term B is the NEP due to shot noise on the bulk leakage current. Term C is the NEP due to the preamplifier noise in addition to surface leakage shot noise of the photodiode.

The circuit of the preamplifier used for the NEP measurements is shown in Figure 24. The amplifier has a current-to-voltage transimpedance of 2.6K over the bandwidth from 3 kHz to 30 MHz. Low-frequency cutoff is due to a coupling capacitor not shown in the schematic. The preamplifier was followed by an HP No. 461 amplifier. The gallium arsenide light-emitting diode was modulated at 40 kHz with  $m = 0.5$ . Provision was made for turning off the modulation without affecting the dc component of light. Output noise and signal were measured on a true rms voltmeter. Using neutral-density filters, the light level on the diode was so adjusted that the S/N ratio was one, or there was 3 dB of difference in output voltage with and without the ac modulation. With this condition met, the output signal voltage was referred to the input and the NEP was calculated from this, knowing  $m$ ,  $\Delta f$ ,  $E_p$ , and  $\eta_a$ . The results are seen in Figure 25 for diode No. 15. The NEP decreases directly with  $M$  until it nulls at a factor of 100 lower than the  $M = 1$  or conventional detector case. Above this null the avalanche noise becomes predominant, and there is an increase in the NEP. The null occurs at an optimum gain of 160 to 200.

Each of the terms A, B, and C, and the NEP from Equation (19), are also shown in Figure 25 in an attempt to correlate the experimental results with the theory. The parameters used in the NEP calculation are:

$$\begin{aligned} E_p &= 1.4 \text{ eV} \\ \eta_o &= 0.9 \\ \eta_a &= 0.4 \\ \Delta f &= 46.2 \text{ MHz} \\ m &= 0.631 \end{aligned}$$

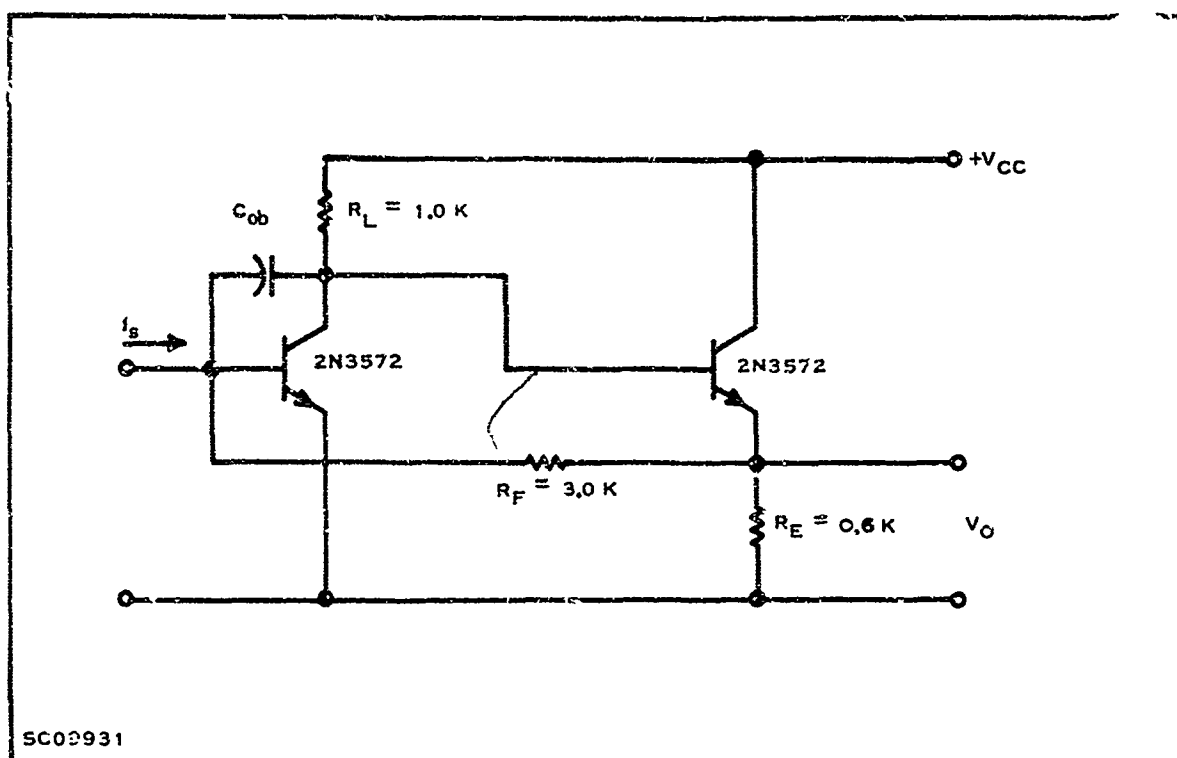


Figure 24. Preamplifier Circuit

$$d = 2.5$$

$$I_{CO} = 0.276 \text{ nA.}$$

Two discrepancies are observed between the measured and the calculated NEP: 1) The magnitude of the minimum NEP and 2) the slope of the NEP at gains greater than the optimum gain. The fact that the measured NEP was lower than the calculated NEP by a factor of 2.5 suggests that the value for  $d$  used in the calculations was too high. Had  $d$  been 2.2 the magnitude of the null would have been the same as that measured.

The major discrepancy is the shape of the NEP at high gains above the null. Theory supports the prediction that NEP in this range will increase with  $M^{d-2}$ ; however, the data show NEP increasing with  $M$  to  $M^2$ , indicating that  $d$  would be 3 to 4. While this is not completely unreasonable, it would require that

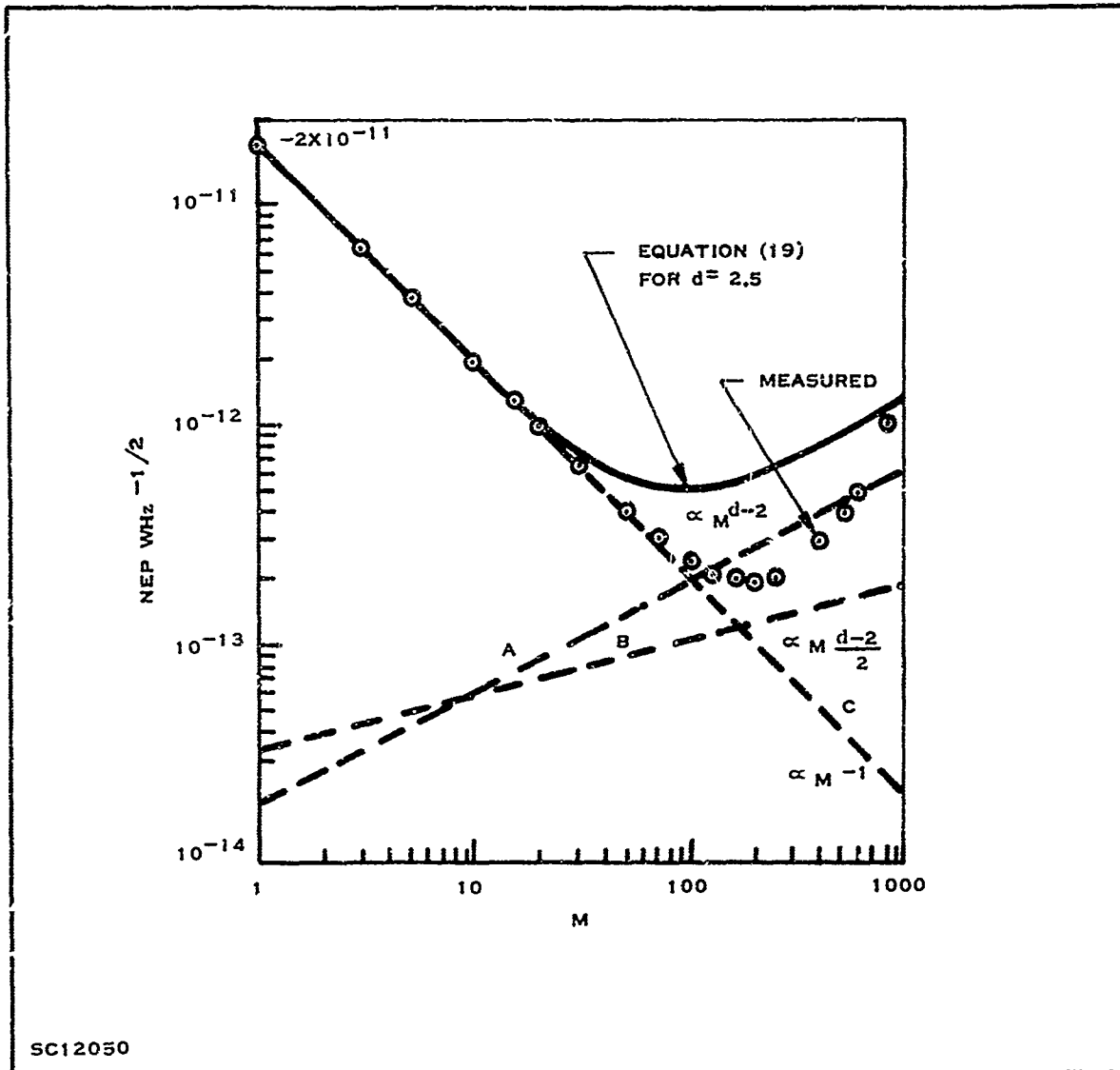


Figure 25. NEP versus Gain for Diode No. 15

the value of A and B at  $M = 1$  would be reduced two orders of magnitudes. Although there could be some error in A or B, it is not at all this large.

One possible explanation for the large slope of NEP above the null resulted from an investigation of the measurement technique. There could be a small amount of ripple or stray pickup on the dc bias side of the diode terminals. At large gains



the diode impedance decreases and a current is fed into the preamplifier. When introduced into the NEP analysis there is an additional term which increases as  $M^2$ . For the NEP magnitude observed at  $M = 500$  the ripple or stray pickup would have to be 0.01 percent of the dc bias voltage. It would also have to be a frequency in the passband of the amplifier. This effect should be studied further for better correlating the measured with the calculated NEP, and also so that some specifications can be put on the avalanche photodiode voltage supplies.

One other possible explanation for the NEP slope above the null is that the diode had a microplasma which became noisy at high gains. This is unlikely because of the smooth curve. Figure 26 shows the measured NEP for diode No. 18, which had a microplasma breakdown at  $MT = 200$ . Note the sharp increase in the NEP as opposed to the gradual increase of diode No. 15.

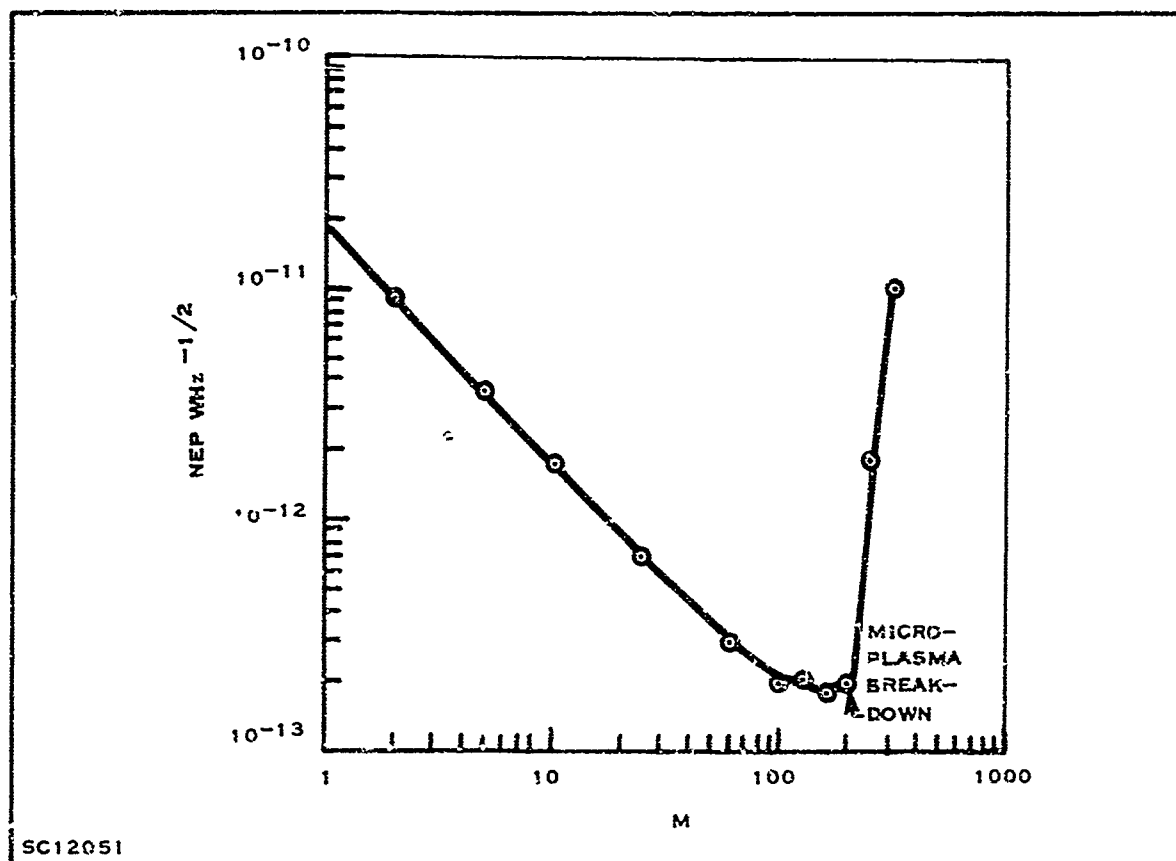


Figure 26. Measured NEP versus Gain for Diode No. 18

Although there is some discrepancy in the NEP data, it is clear that detector sensitivity was substantially improved by using avalanche breakdown. It should be pointed out that in NEP, as normally used,  $m$  is 1.0. For that case the NEP would have been somewhat lower than the measured  $2 \times 10^{-13} \text{ W Hz}^{-1/2}$ .

### 3. Project Performance and Schedule

Texas Instruments Incorporated

Contract No. NObsr 95337 (Report) Date: November 1967

Period Covered: 16 May 1966 through 30 September 1967

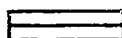
	1966					1967									
	A	S	O	N	D	J	F	M	A	M	J	J	A	S	O
1. Device Design and Fabrication															
Obtain Photomask															
Determine Optimum Diffusions															
Produce Experimental Epitaxial Slices															
Fabricate Planar Epitaxial Diodes															
Fabricate N <sup>+</sup> P Diodes															
2. Characterization of Experimental Diodes															
Gain Characteristics															
Quantum Efficiency															
Noise Performance															
Frequency Response															
3. Characterize and Deliver State-of-the-Art Samples															

SC07948A

Legend:



Work Performed



Schedule of Projected Operation

Item: Estimated completion in percent of total effort expected to be expended (not chronological):

1)	Obtain Photomasks	100%
2)	Determine Optimum Diffusions	100%
3)	Produce Experimental Epitaxial Slices	100%
4)	Fabricate Planar Epitaxial Diodes	100%
5)	Determine Gain Characteristics	100%
6)	Determine Quantum Efficiency	100%
7)	Determine Noise Characteristics	100%
8)	Determine Frequency Response	100%
9)	Characterize and Deliver Samples	100%

Notes and Remarks:

None.

#### D. CONCLUSIONS

The contract was concluded with the successful fabrication and characterization of 20 state-of-the-art silicon avalanche photodiodes. Two types of structures were investigated during the contract period. The NP $\pi$ P structure, first investigated, was found to have edge breakdown in wide  $\pi$ -region diodes. Because of problems with the NP $\pi$ P structure, the N $^+$ P structure utilizing a graded guardring was fabricated.

Final characterization was done on the N $^+$ P diodes. In summary the diodes typically had low-noise gains in excess of 1000, noise slopes of 2.5 and less, series resistance of 50 ohms, junction capacitance of 1.3 pF, ac quantum efficiency of 35 percent at 0.9  $\mu$ m, and bulk leakage currents of 0.5 nA. These parameters result in an NEP of a photodetector system in the order of  $10^{-13}$  W Hz $^{-1/2}$  at 0.9  $\mu$ m and a bandwidth of 30 MHz, a factor of 100 improvement over a non-avalanche system.

SECTION II  
PROGRAM FOR NEXT INTERVAL

With the successful completion of the contract requirements  
the effort has been terminated.

SECTION III

REFERENCES

1. First Interim Engineering Report, Contract No. NObsr 95337, Electronics Division, Bureau of Ships, Navy Department (Dec. 1966).
2. C. O. Thomas et al., "Impurity Distribution in Epitaxial Silicon Films," *Journal of Electrochemical Society*, Vol. 109, No. 11 (Nov. 1962).
3. S. M. Sze and G. Gibbons, "Effect of Junction Curvature on Breakdown Voltage in Semiconductors," *Solid State Electronics*, Vol. 9, pp. 831-845 (1966).
4. S. L. Miller, "Ionization Rates for Holes and Electrons in Silicon," *Phys. Rev.*, Vol. 105, pp. 1246-1249 (February 1957).
5. W. N. Shaunfield et al., "A Germanium Avalanche Photodetector for 1.06 Microns." Presented at the International Electron Devices Meeting, Washington, D.C. (October 1967).
6. W. C. Dash and R. Newman, "Intrinsic Optical Absorption in Single-Crystal Germanium and Silicon at 77°K and 300°K," *Phys. Rev.*, Vol. 99, pp. 1151-1155 (August 1955).
7. C. Sah, R. N. Noyce, W. Shockley, "Carrier Generation and Recombination in P-N Junctions and P-N Junction Characteristics," *Proc. IRE*, pp. 1228-1243 (September 1957).
8. R. J. McIntyre, "Multiplication Noise in Uniform Avalanche Diodes," *IEEE Trans. on Electron Devices*, Vol. ED-13, No. 1, pp. 164-168 (January 1966).
9. H. Melchoir and W. T. Lynch, "Signal and Noise Response of High-Speed Germanium Avalanche Photodiodes," *IEEE Trans. on Electron Devices*, Vol. ED-13, No. 12, pp. 829-838 (December 1966).
10. W. Shockley, "Problems Related to P-N Junctions in Silicon," *Solid State Electronics*, Vol. 2, pp. 35-67 (January 1961).
11. W. W. Gartner, "Depletion-Layer Photoeffects in Semiconductors," *Phys. Rev.*, Vol. 116, pp. 84-87 (October 1959).
12. R. B. Emmons, "Avalanche Photodiode Frequency Response," *Journal of Applied Physics*, Vol. 38, No. 9, pp. 3705-3714 (August 1967).
13. James R. Biard and W. N. Shaunfield, "A Model of the Avalanche Photodiode," *IEEE Trans. on Electron Devices*, Vol. ED-14, No. 5, pp. 233-38 (May 1967).

Unclassified  
Security Classification

DOCUMENT CONTROL DATA - R&D		
(Security classification of title, body of abstract and indexing annotation must be entered when the overall report is classified)		
1. ORIGINATING ACTIVITY (Corporate author) Texas Instruments Incorporated Dallas, Texas, 75222		2a. REPORT SECURITY CLASSIFICATION Unclassified 2b. GROUP
3. REPORT TITLE Development and Fabrication of Solid-State High-Speed Optical Detectors		
4. DESCRIPTIVE NOTES (Type of report and inclusive dates) Final Engineering Report 16 May 1966 through 30 September 1967		
5. AUTHOR(S) (Last name, first name, initial) Shaunfield, Wallace N.		
6. REPORT DATE November 1967	7a. TOTAL NO. OF PAGES 47	7b. NO. OF REFS 13
8a. CONTRACT OR GRANT NO. NObsr 95337 b. PROJECT NO. SF021-02-01 c. d.	9a. ORIGINATOR'S REPORT NUMBER(S) 03-67-104 9b. OTHER REPORT NO(S) (Any other numbers that may be assigned this report)	
10. AVAILABILITY/LIMITATION NOTICES		
11. SUPPLEMENTARY NOTES	12. SPONSORING MILITARY ACTIVITY Navy Department, Bureau of Ships, Electronics Division	
13. ABSTRACT <p>The development, fabrication, and characterization of a high-speed silicon avalanche photodiode for <math>0.9 \mu\text{m}</math> are described. Two structures, an NP<sup>+</sup>P and a graded-guardring N<sup>+</sup>P structure, were fabricated. On the planar NP<sup>+</sup>P structure, edge breakdown was found to be a problem of structures having wide <math>x</math>-regions. Since wide depletion layer widths are required for high ac quantum efficiency at <math>0.9 \mu\text{m}</math>, effort was shifted entirely to the N<sup>+</sup>P structure.</p> <p>Final characterization showed that all the N<sup>+</sup>P diodes delivered had low-noise avalanche gains greater than 160, with many diodes exhibiting gains greater than <math>10^3</math>. The diodes typically have a series resistance of 50 ohms, junction capacitance of 1.3 pF, noise slope of 2.5 or less, ac quantum efficiency of 35 percent, bulk leakage current of 0.5 nA, and a breakdown voltage of 170 volts. The NEP of a 30-MHz bandwidth photodetector system was found to measure <math>2 \times 10^{-13} \text{ W Hz}^{-1/2}</math> at an optimum gain of 160--a factor of 100 improvement over a non-avalanching photodetector.</p>		

DD FORM 1473  
1 JAN 64

Unclassified  
Security Classification

14 KEY WORDS	LINK A		LINK B		LINK C	
	ROLE	WT	ROLE	WT	ROLE	WT
High-speed photodetector Avalanche photodiode Silicon photodetector Low-noise photodiode						

**INSTRUCTIONS**

1. **ORIGINATING ACTIVITY:** Enter the name and address of the contractor, subcontractor, grantee, Department of Defense activity or other organization (*corporate author*) issuing the report.

2a. **REPORT SECURITY CLASSIFICATION:** Enter the overall security classification of the report. Indicate whether "Restricted Data" is included. Marking is to be in accordance with appropriate security regulations.

2b. **GROUP:** Automatic downgrading is specified in DoD Directive 5200.10 and Armed Forces Industrial Manual. Enter the group number. Also, when applicable, show that optional markings have been used for Group 3 and Group 4 as authorized.

3. **REPORT TITLE:** Enter the complete report title in all capital letters. Titles in all cases should be unclassified. If a meaningful title cannot be selected without classification, show title classification in all capitals in parenthesis immediately following the title.

4. **DESCRIPTIVE NOTES:** If appropriate, enter the type of report, e.g., interim, progress, summary, annual, or final. Give the inclusive dates when a specific reporting period is covered.

5. **AUTHOR(S):** Enter the name(s) of author(s) as shown on or in the report. Enter last name, first name, middle initial. If military, show rank and branch of service. The name of the principal author is an absolute minimum requirement.

6. **REPORT DATE:** Enter the date of the report as day, month, year, or month, year. If more than one date appears in the report, use date of publication.

7. **TOTAL NUMBER OF PAGES:** The total page count should follow normal pagination procedures, i.e., enter the number of pages containing information.

8. **NUMBER OF REFERENCES:** Enter the total number of references cited in the report.

9. **CONTRACT OR GRANT NUMBER:** If appropriate, enter the applicable number of the contract or grant under which the report was written.

10. **PROJECT NUMBER:** Enter the appropriate military department identification, such as project number, project number, system numbers, task number, etc.

11. **ORIGINATOR'S REPORT NUMBER(S):** Enter the official report number by which the document will be identified and controlled by the originating activity. This number must be unique to this report.

12. **OTHER REPORT NUMBER(S):** If the report has been assigned any other report numbers (either by the originator or by the sponsor), also enter this number(s).

13. **AVAILABILITY/LIMITATION NOTICES:** Enter any limitations on further dissemination of the report, other than those imposed by security classification, using standard statements such as:

- (1) "Qualified requesters may obtain copies of this report from DDC."
- (2) "Foreign announcement and dissemination of this report by DDC is not authorized."
- (3) "U. S. Government agencies may obtain copies of this report directly from DDC. Other qualified DDC users shall request through \_\_\_\_\_."
- (4) "U. S. military agencies may obtain copies of this report directly from DDC. Other qualified users shall request through \_\_\_\_\_."
- (5) "All distribution of this report is controlled. Qualified DDC users shall request through \_\_\_\_\_."

If the report has been furnished to the Office of Technical Services, Department of Commerce, for sale to the public, indicate this fact and enter the price, if known.

11. **SUPPLEMENTARY NOTES:** Use for additional explanatory notes.

12. **SPONSORING MILITARY ACTIVITY:** Enter the name of the departmental project office or laboratory sponsoring (paying for) the research and development. Include address.

13. **ABSTRACT:** Enter an abstract giving a brief and factual summary of the document indicative of the report, even though it may also appear elsewhere in the body of the technical report. If additional space is required, a continuation sheet shall be attached.

It is highly desirable that the abstract of classified reports be unclassified. Each paragraph of the abstract shall end with an indication of the military security classification of the information in the paragraph, represented as (TS), (S), (C), or (U).

There is no limitation on the length of the abstract. However, the suggested length is from 150 to 225 words.

14. **KEY WORDS:** Key words are technically meaningful terms or short phrases that characterize a report and may be used as index entries for cataloging the report. Key words must be selected so that no security classification is required. Identifiers, such as equipment model designation, trade name, military project code name, geographic location, may be used as key words but will be followed by an indication of technical context. The assignment of links, rules, and weights is optional.